Mechanics of Materials 186 (2023) 104810

Contents lists available at ScienceDirect

Mechanics of Materials

journal homepage: www.elsevier.com/locate/mecmat

Research paper

Computational modeling of viscoelastic backsheet materials for photovoltaics

A.R. Dusane *, P. Lenarda, M. Paggi

IMT School for Advanced Studies Lucca, Piazza San Francesco, 19, 55100 Lucca, Italy

ARTICLE INFO

Keywords:
Prony series model
Fractional calculus model
Creep
Relaxation modulus
Linear viscoelasticity

ABSTRACT

Backsheet is the outermost layer of the photovoltaic (PV) laminate which consists of polymers such as Polyethylene terephthalate (PET) or Polyvinyl fluoride (PVF). The viscoelastic response of these materials significantly affects the durability of the PV module. In this study, the viscoelastic response of commercially available backsheet materials is experimentally characterized and computationally modeled. An extensive viscoelastic experimental study on backsheet materials is carried out, considering the temperature-dependent properties to characterize the mechanical properties. Based on an experimental campaign, small-strain viscoelastic models based on the Prony-series (PS) and Fractional Calculus (FC) are herein proposed. The form of the constitutive equations for both models is outlined, and the finite element implementation is described in detail. Following the identification of the relevant material parameters, models are validated with experimental data, showing good predictability. A comparative study of model responses under different loading conditions is also reported to assess the advantages and disadvantages of both models. Such an extensive experimental study and constitutive modeling will help design and simulate a more comprehensive digital-twin model of PV modules, as illustrated by the benchmark problems.

1. Introduction

Photovoltaic (PV) modules are laminates composed of thin layers, as schematically shown in Fig. 1. The durability of PV modules has always been a subject of concern (Kim et al., 2021; Paggi et al., 2016), primarily because of their multilayered structure. Various material degradation mechanisms have been discussed in the literature to understand the origin of the PV module's overall underperformance (Liu et al., 2019). The mechanical and electrical response of PV modules may degrade over time due to various environmental factors, such as humidity, solar radiation, temperature, and external loading, causing mechanical damage in Silicon solar cells in the polymeric materials (Vázquez and Rey-Stolle, 2008; Borri et al., 2018; Liu et al., 2022). Developing a comprehensive multiphysics model that can predict the overall mechanical behavior of PV modules under different conditions is still an active area of research (Omazic et al., 2019). Till now, the scientific community has given more attention to EVA (Poly-ethylene Vinyl Acetate), which encapsulates the silicon solar cells (Czanderna and Pern, 1996). The EVA mechanical properties, its chemical and physical degradation, and its response to temperature are widely known (De Oliveira et al., 2018; Gagliardi et al., 2017) and, in most cases, they have been successfully modeled (Hirschl et al., 2013; Gagliardi et al., 2017). On the other hand, much less attention has been given to the experimental characterization and modeling of the backsheet materials, which are used for the outermost layer of the PV module. Several commercial types are available with very different physico-mechanical characteristics. The primary purpose of the backsheet is to protect the inner components of the module, specifically the Silicon solar cells and electric components, from external loading and also to act as an electric insulator. Therefore, any damage may cause a severe safety hazard. Usually, backsheets are made up of polymers such as Polyethylene terephthalate (PET), Polyvinyl fluoride (PVF), Polyvinylidene fluoride (PVDF), and Polyamide (PA), with thicknesses ranging from 30 to 270 μm.

Analysis of the backsheet mainly emphasized material identification of polymers to be incorporated into the PV module and the determination of material degradation effects/failure analysis, which are based on chemical and material properties of their constituent polymers. These materials often show a complex rheological behavior, changing their properties over time. In most cases, responses of backsheets are modeled within the elastic regime only (Ottersböck et al., 2022). At the same time, there is lack of a complete characterization of their viscoelastic response. The elastic modulus of the backsheet material may vary depending on the temperature and corresponding relaxation time. Similar to EVA and other polymers, backsheet materials also show

* Corresponding author.
E-mail addresses: ajinkya.dusane@imtlucca.it (A.R. Dusane), pietro.lenarda@imtlucca.it (P. Lenarda), marco.paggi@imtlucca.it (M. Paggi).

https://doi.org/10.1016/j.mechmat.2023.104810
Received 21 April 2023; Received in revised form 24 July 2023; Accepted 12 September 2023
Available online 18 September 2023
0167-6636/© 2023 The Author(s). Published by Elsevier Ltd. This is an open access article under the CC BY license (http://creativecommons.org/licenses/by/4.0/).

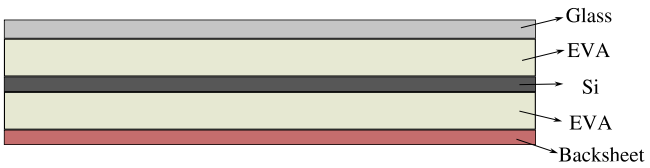

Fig. 1. Schematic representing different components of a PV module.

power-law-type stress relaxation, and their behavior can be studied through viscoelasticity. Backsheet properties significantly influence the stress and deformation state of the PV module (Dietrich et al., 2010).

In order to identify the viscoelastic response of the material, various experimental tests, such as relaxation tests (at a constant applied strain level, stress is recorded) and creep tests (at a constant applied stress level, strain is recorded). Apart from these, Dynamic-Mechanical Analysis (DMA tests) can be used to determine the characteristics of materials efficiently. The latter applies sinusoidal-varying stress and measures the deformation of the material, allowing the determination of the storage modulus as well as the loss modulus. Based on frequency response, viscoelastic material parameters are identified (Bosco et al., 2020). The properties of viscoelastic materials strongly depend on temperature as well. The temperature dependency can be taken into account by means of the Time-Temperature-Superposition-Principle (TTSP) (Kraus et al., 2017), which provides all relaxation/creep functions at a given temperature from the material response at a reference temperature, T_{ref}. In practice, backsheets are often exposed to high temperatures with a load that induces constant stress or strain over a period of time. Therefore, relaxation tests seem to be the most appropriate test for identifying the parameters in relation to the applications.

Various mathematical models have been proposed in the literature to model the viscoelastic response of materials (Taylor et al., 1970; Knauss, 2015). The primary aim of modeling is to extract model parameters and relate them to different deformation mechanisms. The linear viscoelastic model is an integro-differential equation in which the elastic stress tensor is a convolution product between the strain with a time-dependent elastic relaxation modulus. Models based on a combination of springs and dashpots are often used to get exponential-type relations and provide an approximate power-law trend of the elastic parameters' dependence over time. A more versatile Maxwell model proposed by Maxwell and Wiechart (Marques and Creus, 2012) consists of a linear spring and a dashpot in parallel, giving rise to a Generalized Maxwell Model (GMM), also called Prony Series (PS) model, which is used to fit experimental data (Kaliske and Rothert, 1997; Reese and Govindjee, 1998; Simo, 1987). A high number of prony series is often required to improve the fitting accuracy, giving rise to several drawbacks, including the fact that many unknown parameters must be identified (Pander et al., 2011). The PS models are already in use to describe the linear viscoelastic behavior of solids such as polymers (Xu and Engquist, 2018; Eitner, 2011; Sánchez et al., 2022), asphalt concrete (Xu and Solaimanian, 2009), biological materials (Budday et al., 2017), etc. The numerical implementation of the PS models is also computationally convenient due to its exponential format for closed-form solutions in time integration (Chen, 2000; Reese and Govindjee, 1998).

Alternatively, models based on fractional calculus (FC) are becoming a promising alternative to modeling the power-law dependency of the relaxation behavior of polymers (Paggi and Sapora, 2015). As power-law relations rise naturally by assuming a material constitutive law of fractional type, that is, involving noninteger order derivatives of stress and/or strain (Alotta et al., 2018a; Bonfanti et al., 2020). Implementation of FC models is pretty straightforward, as convolution integral can be represented in the form of Caputo fractional derivative (Samko et al., 1993; Alotta et al., 2018b). Recent work by Lenarda and Paggi (2022) shows that fractional calculus offers the easiest way to estimate the model parameters compared to other models.

Based on these premises, the contribution of the current study has the following specific aims. At first, a comprehensive experimental campaign on different types of commercial backsheets to evaluate their material properties, considering uniaxial tensile tests and temperature-dependent relaxation tests, was performed. We have proposed small-strain linear viscoelastic models based on Prony Series or Fractional Calculus to capture the viscoelastic response. So, a valid comparative study can be made. The form of the constitutive equations for both models is summarized in brief, and the finite element implementation is described in detail. Since experimental results are obtained using uniaxial tests, we reformulate the two-dimensional viscoelastic constitutive model to one-dimensional forms. Afterward, all parameters of the models are identified using an optimization procedure with additional focus given to addressing the issue of reducing model parameters. For that reason, a MATLAB program has been written for parameters' identification. Finally, some benchmark problems are discussed to show the capability of the developed models through Finite Element Analysis (FEA).

The manuscript is organized as follows. A brief note describing experimental tests with results carried out in the MUSAM-Lab at the IMT School for Advanced Studies Lucca is presented in Section 2. Section 3 provides an overview of the linear viscoelastic material models herein considered. The proposed Prony Series (PS) and the Fractional Calculus (FC) models are described in detail, and the complexities arising from their parameters' identification are discussed. Moreover, their finite element implementation is described. Section 4 discusses the proposed optimization procedure for parameters' identification and presents the results for the considered backsheets, with a critical perspective regarding the two different viscoelastic models. Section 5 presents the numerical analysis and model validations with previously identified parameters. Finally, concluding remarks close the manuscript in Section 6, with an outlook on future developments.

2. Experimental tests

2.1. Materials' description and properties

The experiments described in this section have been conducted in the MUSAM-Lab of the IMT School for Advanced Studies Lucca. All the specimens were tested with the Zwick/Roell Z010TH universal standard testing machine equipped with a 1 kN load cell and with the Zwick/Roell BW91272 thermostatic chamber to perform the experiments at different imposed temperatures. The detail of the experimental setup is shown in Fig. 2. The thickness of each sample varies according to the respective manufacturer. The details of the material composition and thickness of the tested backsheet specimens are given in Table 1. The backsheet material may be multilayer or single-layer. All backsheet materials under study have antireflective coatings on both sides, for protection. In the present study, rectangular-shaped sample specimens are prepared from a large sheet provided by the manufacturer, with 70 mm × 20 mm dimension, and considering a gauge length of 50 mm. Samples are cut out very carefully using a sharp cutter. Dimensions are chosen such that there would not be any effect from grippers' (edge) effects due to the presence of enhanced areas at sample ends (Hervy et al., 2017). In all experimental results presented, we use nominal stress (PK1), and the corresponding nominal strain corresponds to the change in deformation with respect to the initial length of the gauge section. Fig. 3 shows the confocal photomicrographs of the cross-sections of the different backsheets (taken with the Leica DCM3D confocal microscope), with surface textures or variable roughness on surface sides (a) and (b). The multilayered composition of the OSBS, TPE-HD, and Reflect Lean backsheets can be clearly observed, while Lexan is a monolayer material.

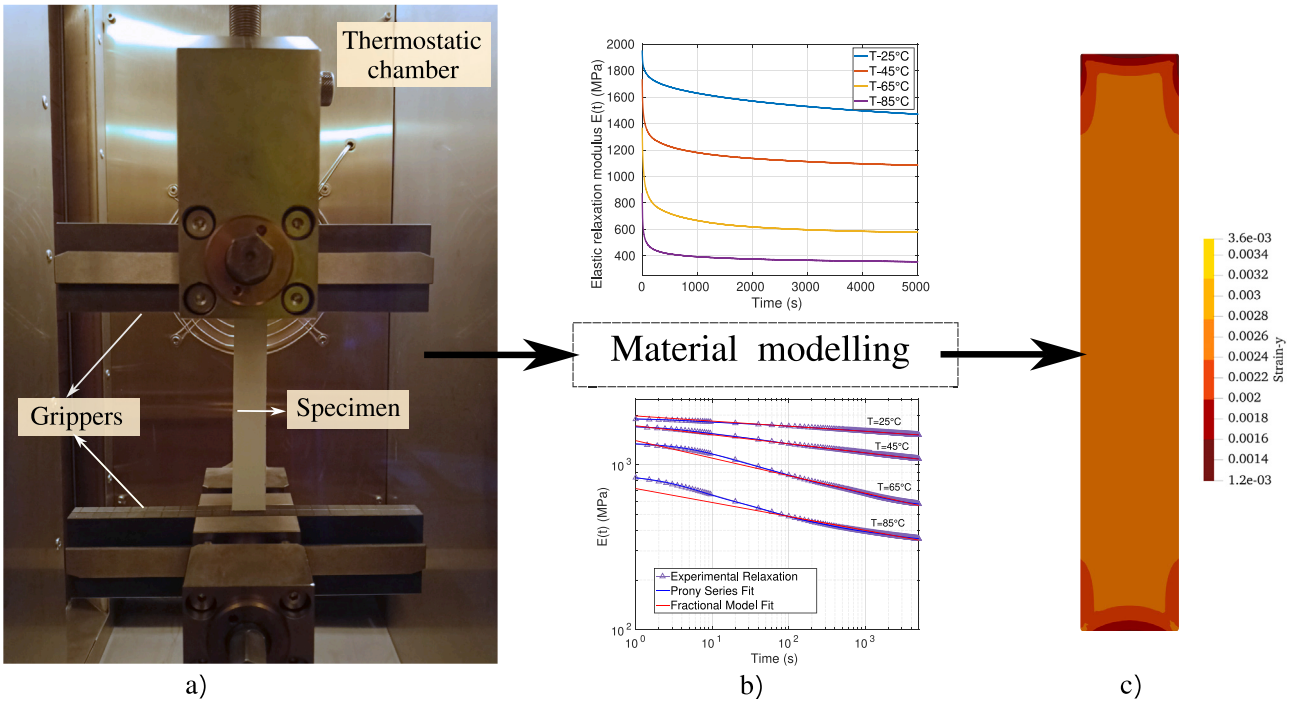

Fig. 2. Schematic illustrating steps in modeling (a) complete experimental setup with the loaded specimen highlighting relevant components (b) Modeling response using Prony Series (PS) or Fractional Calculus (FC), and (c) FEM implementation for simulations.

Table 1
Commercial names and composition of the testing materials.

Commercial Name	Abbreviation	Material composition	Thickness (μm)	Remark
Reflexolar OSBS	OSBS	White PP, polyamide, clear polyester	320	Co-extruded
Madico TPE-HD	TPE-HD	White PVF, clear polyester, EVA	285	Laminated
Medico Reflekt LEAN	Reflekt Lean	Fluoropolymer, polyester, polyolefine	269	Laminated
Lexan FR25A	Lexan	Polycarbonate	297	Monolayer coated

2.2. Uniaxial tensile tests

The uniaxial tensile tests are often performed to determine the strength of materials. Material behavior can be categorized based on the relationship between stress, σ, vs. strain, ϵ. To understand the temperature effect on elasticity, the uniaxial tensile test was performed on the backsheet specimens at an ambient 25°C temperature and at a higher temperature of 85°C, at which viscoelastic effects are more prominent, motivated by some of the standard accelerated ageing tests for the assessment of the durability of PV modules which require high temperatures around 85°C. All backsheets were loaded by applying a constant strain over time. Moreover, uniaxial tests up to failure were carried out with a constant loading rate of 0.1 mm/s at 25°C and at 85°C. Plots of complete uniaxial tensile stress vs. strain are shown in Fig. 4. The backsheet materials, such as TPE-HD and ReflektLean, show plastic behavior before failure. The elastic modulus is calculated considering small strains up to 0.02 (2%), which is a conventional assumption. The response becomes non-linear as strains start increasing further. A common observation is that the load-bearing capacity of backsheet materials has decreased at 85°C as compared to the ambient temperature. As backsheets are made of polymers, the load required to straighten up the complex polymer chain at high temperatures decreases, directly affecting their strength. The strength of Lexan was found to be the highest, irrespective of temperature. The strength of OSBS was found to be the lowest. The response fitted linearly within the limit of 0.02 strain to find the elastic modulus under finite deformations. The bar chart compares elastic moduli for materials represented as shown in Fig. 5. The measured strength values for all the materials are collected in Table 2.

Table 2
Evaluated tensile strength of backsheet materials.

Material	σ_{25} (MPa)	σ_{85} (MPa)
OSBS	4.57	0.6158
TPE-HD	38.12	22.10
ReflektLean	26.48	13.14
Lexan	42.66	37.78

In the literature, Romer et al. (2020) and Lang et al. (2022) observed that the coefficient of thermal expansion (CTE) change due to anisotropy of backsheet layers. The anisotropic nature of films may arise due to the manufacturing process. Here, we performed uniaxial tests with specimens cut along two orthogonal directions, to check anisotropy effects. Results, not reported here, do not show significant anisotropic effects on the stress–strain diagrams for the considered backsheets, which are therefore modeled via an equivalent single-layer material.

2.3. Relaxation tests

Following the experimental analysis performed by Eitner (2011) and Borri et al. (2018), at 85 °C, the backsheet material experiences thermal stresses around 4–8 MPa, which is sufficient enough to support viscoelastic straining/relaxation effects. Therefore, a series of relaxation tests were performed by holding the sample at corresponding constant strains for a long duration of time at a given temperature. In the current study, relaxation tests were carried out at different

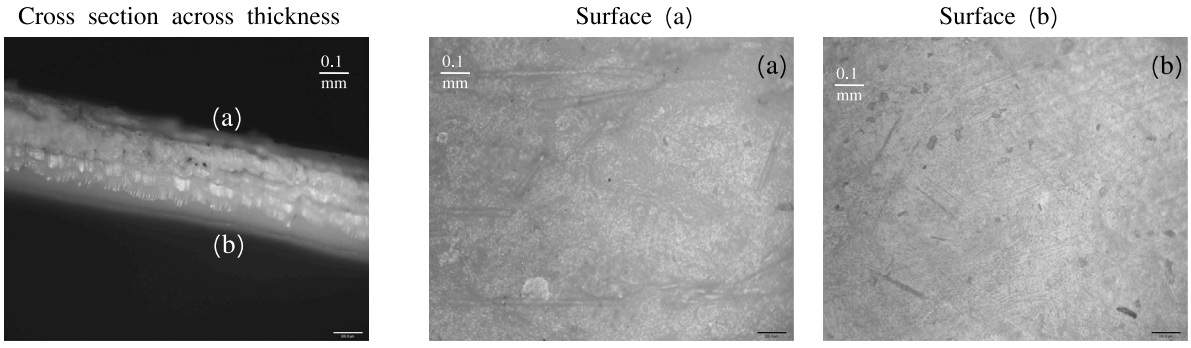

(a) OSBS Co-extruded multilayered backsheet

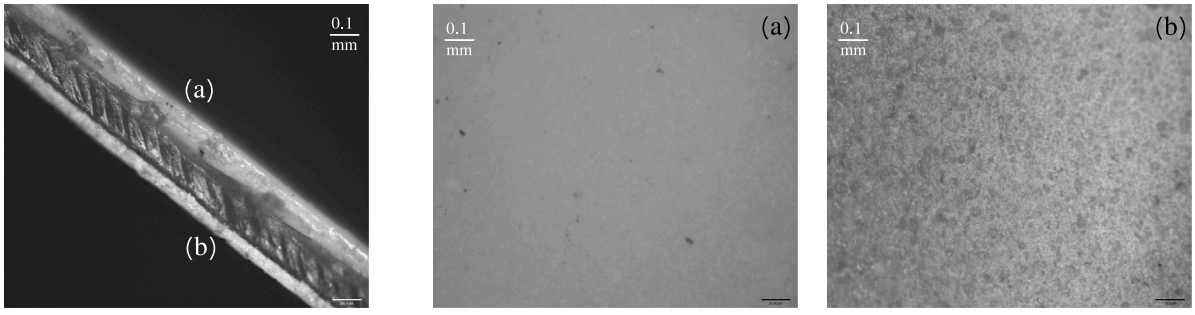

(b) TPE-HD multilayered laminated backsheet

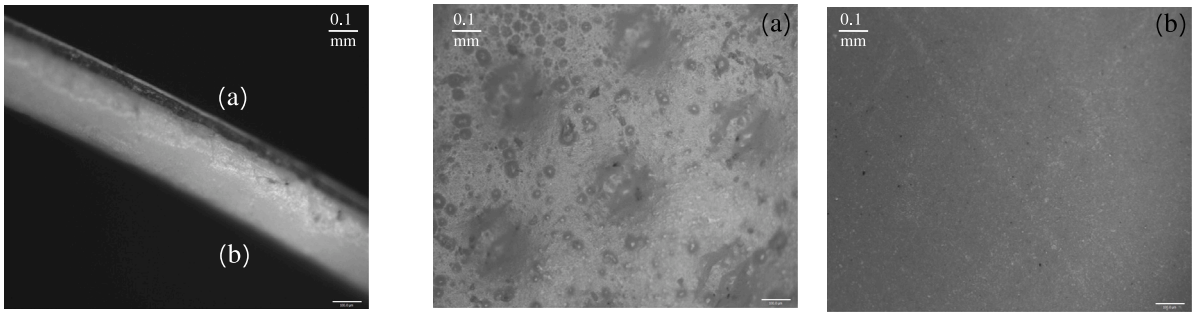

(c) Reflect Lean multilayered laminated backsheet

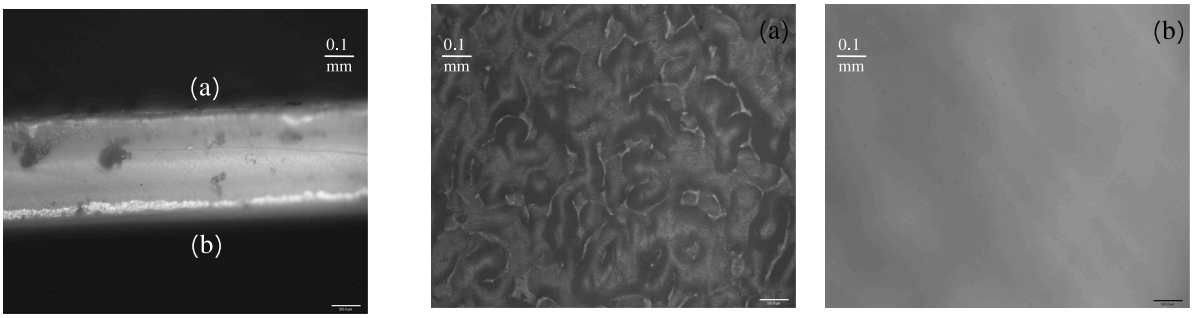

(d) Lexan monolayer coated backsheet

Fig. 3. Confocal photomicrograph of a cross-section of backsheets and their surfaces on sides (a) and (b), using the Leica DCM3D confocal profilometer, 10x magnification. The multilayered structure is clearly observed for OSBS, TPEHD, and Lean backsheets, whereas Lexan is monolayered. Surfaces on sides (a) and (b) present different level of roughness and sometimes texture, to facilitate bonding.

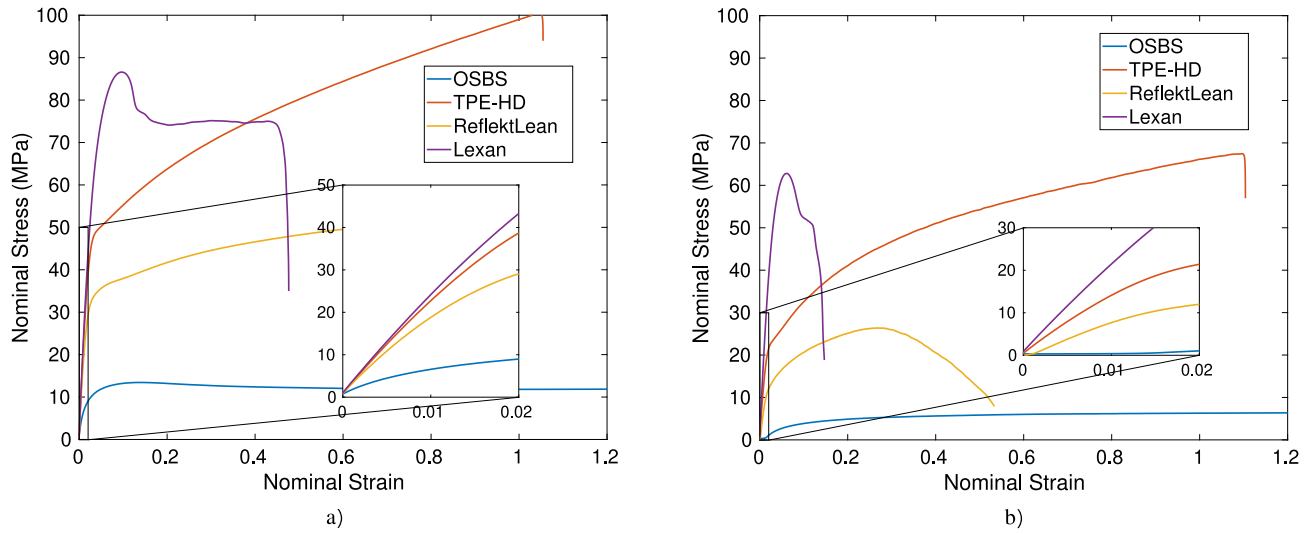

Fig. 4. Tensile test performed until failure of specimens loaded with 0.1 mm/s at (a) 25 °C and (b) 85 °C respectively.

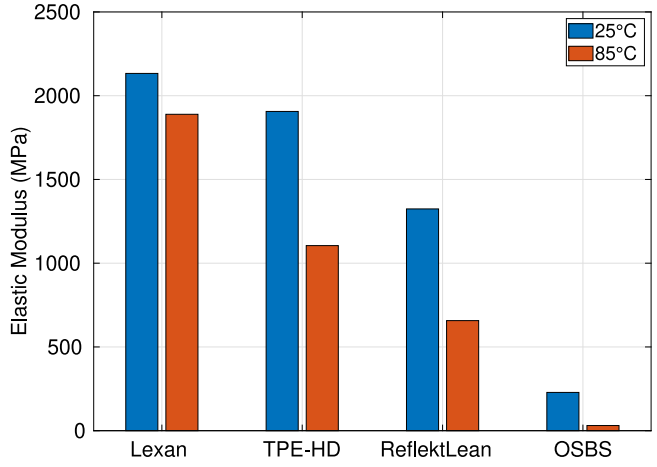

Fig. 5. Bar chart comparing elastic modulus of backsheets.

temperatures in the range 25–85 °C, to investigate temperature effects. The initial loading rate was kept constant until all cases reached the corresponding strain, using 0.1 mm/sec. We have kept the initial loading rate constant so that results will align with uniaxial tests and valid comparisons can be carried out. The instantaneous elastic modulus can be estimated by considering the problem as one-dimensional $E_{ins} = \sigma/\epsilon_0$. Corresponding values are collected in the Table 3. The values of the instantaneous elastic moduli are very much within the range of elastic moduli estimated previously from the tensile test. Fig. 6 shows the relaxation response of the Lexan backsheet at corresponding temperatures. Instantaneous elastic modulus reduces as temperature increases. The relaxation response of other materials is represented in Fig. 7. All materials except OSBS follow the power-law type relaxation behavior at higher temperatures. As OSBS has the lowest elastic strength compared to others, it relaxes faster. A backsheet is a layered composition of different polymeric materials. Every material has its own glass transition T_g, which affects the total relaxation response. As OSBS consists of polyamide (PA) and polyethylene(PE) polymers, which have respective T_g which is lower than other materials as shown in Table 4, it loses its power law relaxation behavior as temperature goes higher than 45 °C. As this study is performed at a specific operating range of temperatures, it is difficult to comment on glass temperature for a complete backsheet. But, It can be seen that other backsheet materials show the power law until 85 °C. These backsheet materials have T_g higher than 85 °C. These elastic relaxation responses of backsheet materials can be modeled using different material models.

The relaxation tests were performed on Lexan specimens at a constant temperature for different strain levels to assess how the maximum applied strain affects relaxation. Fig. 8 shows the relaxation response for different constant strains $\epsilon = 0.0167, 0.0250$, and 0.0333, for Lexan at 85 °C. Initially, stress is proportional to strain, but the response becomes nonlinear for higher strains. It is noted that at higher temperatures, specimens loaded at small strains relax faster than compared to what happens at larger strains. The study is performed to see changes in material relaxation parameters for different strains at constant temperature which is discussed in Section 4.

3. Constitutive modeling of small-strain viscoelasticity

Viscoelastic materials are characterized by their Relaxation and Creep functions $R(t)$ and $C(t)$, respectively. These functions describe the behavior of the material when a constant strain or a constant stress is applied, respectively. Depending upon the choice of creep and relaxation response fitting with experimental tests, these functions can be modeled with exponential functions (PS model) or power-law functions (FC model) as given below:

$$R(t) = E_\infty + \sum_{j=1}^{N} E_j e^{-\frac{t}{\tau_j}}; \qquad C(t) = \frac{1}{E_\infty} + \sum_{j=1}^{N} \frac{1}{E_j}\left[1 - e^{-\frac{t}{\tau_j}}\right] \tag{1}$$

$$R(t) = \frac{A_\alpha t^{-\alpha}}{\Gamma(1-\alpha)}; \qquad C(t) = \frac{t^\alpha}{A_\alpha \Gamma(1+\alpha)} \tag{2}$$

where E_∞ and E_i are materials parameters for relaxation moduli corresponding to the fixed spring and the ith spring of Maxwell's arm in the PS model, whereas $\Gamma(\cdot)$ is the Euler gamma function, α is a real number $0 \le \alpha \le 1$, and A_α is a material parameter. All these material parameters are evaluated by fitting creep or experimental relaxation curves. The constitutive models can be represented with physical means as shown in Fig. 9. In the linear viscoelasticity framework, the Boltzmann superposition principle allows us to obtain the response of a material when the imposed stress $s(t)$ or strain history $e(t)$ is not constant and can be expressed in two forms:

$$s(t) = \int_0^t R(t-\tau)\dot{e}(\tau)d\tau \tag{3}$$

$$e(t) = \int_0^t A(t-\tau)\dot{s}(\tau)d\tau \tag{4}$$

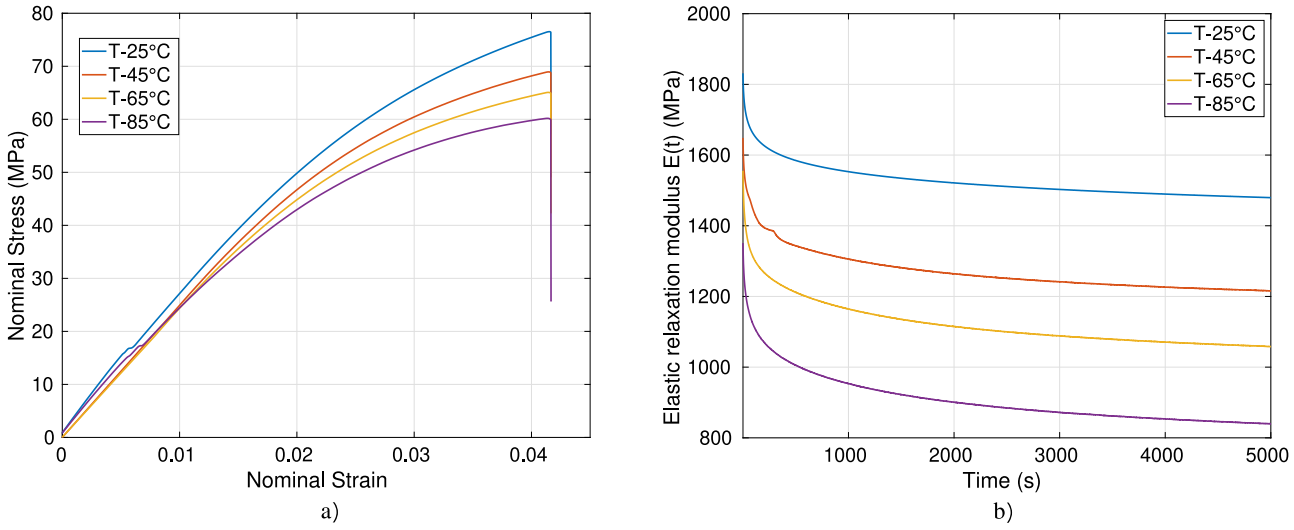

Fig. 6. Temperature-dependent relaxation test response of Lexan backsheet: (a) Nominal stress over nominal strain, and (b) change in the elastic relaxation modulus over time (s).

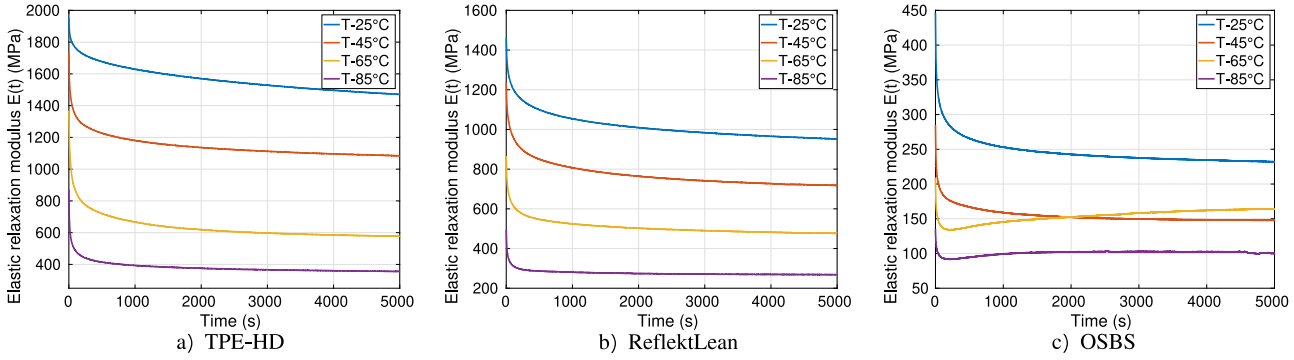

Fig. 7. Temperature dependent relaxation test: response of change in the elastic relaxation modulus over time (s) for (a) TPE-HD, (b) Lean, and (c) OSBS backsheet materials respectively.

Table 3
Instantaneous elastic modulus for the backsheet materials at the start of relaxation, for each corresponding test temperature.

Material	Strain (ϵ_0)	E_{25} (MPa)	E_{45} (MPa)	E_{65} (MPa)	E_{85} (MPa)
OSBS	0.02	446.18	285.2	175.68	135.43
TPE-HD	0.02	1914.9	1735.8	1368.7	874.31
RefelektLean	0.02	1462.8	1236.7	866.47	495.03
Lexan	0.0417	1836.6	1654.6	1561.8	1444.3

Table 4
Composition of backsheet materials with respective thicknesses and glass transition temperatures (T_g).

Material	Layer composition	Thickness (μm)	T_g (°C)
OSBS	OSBS	160	–
	White formulated PP	10	(−20,−10) (Omnexus)
	White PA	40	(35,50) (Omnexus)
	White/Transparent PE	30	(−110,−130) (Fred-Ahmadu et al., 2020)
Lexan	Polycarbonate	297	(150,160) (Omnexus)
TPE-HD	White PVF	37.5	(120,130)(Polymerdatabse)
	Polyester	127	(70,90) (Fred-Ahmadu et al., 2020)
	Laminating Adhesives	–	–
	EVA	110	(−40,−30) (Agroui et al., 2012)
Reflekt Lean	Fluoropolymer	10	–
	Polyester	51	(70,90) (Fred-Ahmadu et al., 2020)
	Laminating Adhesives	–	–
	Polyolefin	203	(120,160) (Henschke et al., 1997)

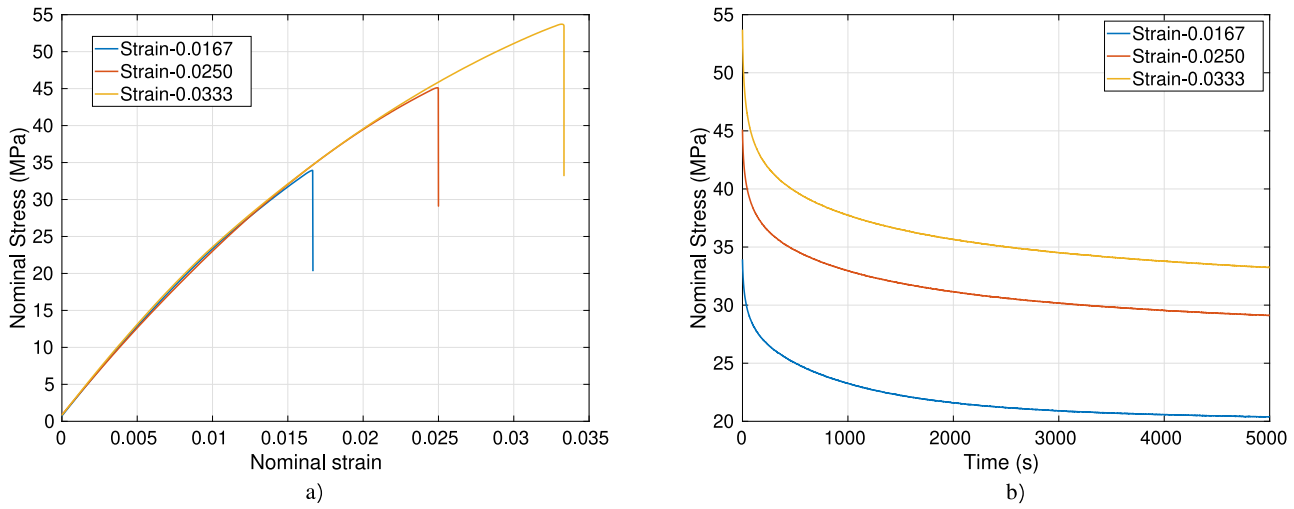

Fig. 8. Relaxation test response of Lexan backsheet at constant temperature: (a) Nominal stress vs. nominal strain, and (b) elastic relaxation modulus vs. time (s).

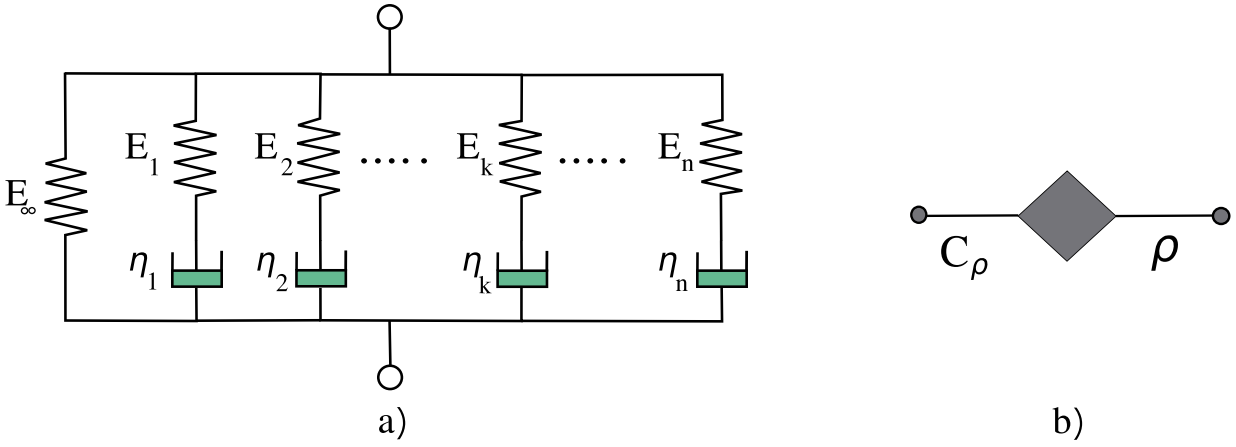

Fig. 9. Schematic of representation (a) Generalized Maxwell Model (b) Spring-pot Model for viscoelastic material models.

These integrals are called hereditary integrals because the actual value of $s(t)$ (or $e(t)$) depends on the previous history of $e(t)$ (or $s(t)$). Substitution of Eqs. (1) and (2) into the above Eqs. gives the corresponding constitutive law. Let us consider any solid body occupying region $\Omega \subset \mathbb{R}^{n_{\text{dim}}}$ ($n_{\text{dim}} = 1, 2, 3$ spatial dimensions). Let $\mathbf{u}$ be the displacement field. Corresponding strain field can be defined as $\varepsilon := \text{sym}(\nabla \mathbf{u})$. The external boundary $\partial\Omega \subset \mathbb{R}^{n_{\text{ndim}}-1}$ composed of two open, disjoint regions, $\partial\Omega = \overline{\partial\Omega_u \cup \partial\Omega_t}$ such that $u = \bar{u}$ on $\partial\Omega_u$ and $t = \bar{t}$ on $\partial\Omega_t$. For such a body, the total energy functional can be given as:

$$\Pi := \int_{\Omega} \Psi(\varepsilon)\, \mathrm{d}\Omega - \int_{\Omega} f_v \cdot u\, \mathrm{d}\Omega - \int_{\partial\Omega} \bar{t} \cdot u\, \mathrm{d}\partial\Omega \tag{5}$$

Where f_v is a body force and $\Psi(\varepsilon)$ is elastic energy density function which is defined as $\Psi(\varepsilon) = \varepsilon(u)^T : \sigma(u)$, where $\sigma(u)$ is the stress which can also be given as $\sigma(u) := \mathbb{C} : \varepsilon(u)$ where $\mathbb{C}$ is a constitutive material tensor that is obtained through different material models. In the current study, we have modeled elastic relaxation response $R(t)$ separately at a given operating temperature (T_{opt} = constant). So, there is no need to consider separate thermal effects in the model formulation.

3.1. Generalized Maxwell model for linear viscoelasticity

The behavior of viscoelastic materials under loading is usually represented by conceptual models composed of elastic and viscous elements which correspond to springs and dashpots. A more general form of this is PS models, where an isolated spring is attached in parallel to several series spring–dashpot models, which are also called Maxwell's arms, to get a better viscoelastic response. The representative model is shown in Fig. 9. As there are 2N+1 unknown parameters required to fit the experimental test, these models can give a good fit compared to other models. However, it can be cumbersome since all the parameters should also have physical meaning rather than just numerical parameters. In most of the implementations, the most convenient choice is to use volumetric $K_R(t)$ and deviatoric relaxation $G_R(t)$ (or creep) functions (Taylor et al., 1970). In the case of the PS model, these functions can be taken as a series of exponential responses similar to Eq. (1) as,

$$G_R(t) = G_\infty + \sum_{j=1}^{N} G_j e^{-\frac{t}{\tau_j^g}}; \qquad K_R(t) = K_\infty + \sum_{j=1}^{N} K_j e^{-\frac{t}{\tau_j^k}} \tag{6}$$

Where, G_∞, G_i and K_∞, K_i are shear and bulk relaxation moduli for the ith Maxwell arm, respectively, with τ_i^g and τ_i^k the corresponding relaxation time periods. Following (Holzapfel and Simo, 1996), bulk relaxation modulus can be taken as constant $K_R(t) = K^v$. This is because polymers show a predominant visco-elastic behavior in shear deformation rather than in volumetric expansion. It also limits the number of unknowns to evaluate. Now, the strain–stress relationship can be given from Eq. (3) as:

$$\bar{\sigma}(t) = \int_0^t R(t-\tau)\dot{\varepsilon}(\tau)\mathrm{d}\tau = K^v\theta + 2\int_0^t G_R(t-\tau)\dot{e}(\tau)\mathrm{d}\tau \tag{7}$$

where ε is the actual strain given as $\varepsilon = \boldsymbol{e} + \frac{1}{3}\theta$, in which $\theta = tr(\varepsilon)\cdot I$ and $\mathbf{e}$ are the corresponding second-order volumetric and deviatoric tensors. K^{υ} is the time-independent bulk modulus, and $\dot{e}(\tau)$ shows the rate of change of deviatoric strains with time. Following Eq. (6), G_{∞} is the shear modulus in the pure spring batch, which is also called the long-term shear modulus, and N denotes the number of Maxwell's arms. The term $\tau_i = \eta_i/\mu_i$ (μ_i is the shear modulus) is the relaxation time for each dashpot branch, which controls the time it takes for the stress to relax (the higher τ_i, the longer the stress relaxation times); η_i is the viscosity of the ith dashpot, which basically defines the strain rate dependence of material which can be taken as constant. The deviatoric stress $\bar{\sigma}_{dev}(t)$ from Eq. (7) can be written as:

$$\bar{\sigma}_{dev}(t) = 2G_{\infty}e(t) + \sum_{i=1}^{N} 2\int_0^t G_i e^{-\frac{t-\tau}{\tau_i}}\dot{e}(\tau)\mathrm{d}\tau \tag{8}$$

Using the time integration scheme for implementation of semi-analytical integration of the convolution integral, which is presented in (Taylor et al., 1970) and (Londono et al., 2016), the deviatoric stress $\bar{\sigma}_{dev}(t)$ at time $n+1$ for a time step of Δt can be written in the form differential operators as:

$$\bar{\sigma}_{dev}(t) = 2\left[G_{\infty}e(t) + \sum_{i=1}^{N}\left(G_i \exp\left(-\frac{\Delta t}{\tau_i}\right)h^i_{n+1}\right)\right] \tag{9}$$

where, h^i_{n+1} is the stress corresponding to the ith Maxwell arm at current time $n+1$ which can be given as an update integral considering strains at the current step and previous strains:

$$h^i_{n+1} = \exp\left(-\frac{\Delta t}{\tau_i}\right)h^i_n + h_{\mathrm{vis}}\left(e_{n+1} - e_n\right) \tag{10}$$

Where h^i_n takes care of the previous time-step history of h^i, and h_{vis} is given by

$$h_{\mathrm{vis}} = \frac{\tau_i}{\Delta t}\left(1 - \exp\left(-\frac{\Delta t}{\tau_i}\right)\right) \tag{11}$$

Finally, the constitutive law for viscoelastic solids with moduli in the form of a Prony-series is obtained by substituting Eqs. (10) and (11), into Eq. (7), which gives the total stress $\bar{\sigma}(t)$ in the material. Due to the flexibility of accommodating a number of unknowns, in many cases of engineering interest, the PS models can adequately reproduce the time-dependent features of viscoelastic materials (Knauss, 2015; Xu and Engquist, 2018).

3.2. Fractional calculus model for linear viscoelasticity

The volumetric and the deviatoric creep/relaxation functions are both well-fitted by a pure power-law function. Then their behavior can be reproduced by the spring pot model as shown in Fig. 9. In the case of the fractional calculus model, the substitution of relaxation function $R(t)$ into Eq. (3) leads to constitutive laws that involve fractional operators, namely derivatives and integrals of real order (Samko et al., 1993; Alotta et al., 2018a). It is straightforward in which strain history is applied. Based on that, the corresponding stress history can be given as follows:

$$s(t) = \frac{A_{\alpha}}{\Gamma(1-\alpha)}\int_0^t (t-\tau)^{-\alpha}\dot{e}(\tau)\mathrm{d}\tau = A_{\alpha}D^{\alpha}_t e(t) \tag{12}$$

where D^{α}_t represents the Caputo fractional derivative of order α (Podlubny, 1999; Scherer et al., 2011), i.e., a convolution integral with a power-law kernel. It has been shown in (Paggi and Sapora, 2015) and (Lenarda and Paggi, 2022) that the behavior of the number of springs/dashpots in a classical viscoelasticity framework can be easily reproduced with a spring pot. This is why using fractional viscoelasticity results in a significant reduction of mechanical parameters as compared to classical viscoelastic models. Similar to the PS model, volumetric $K_R(t)$ and deviatoric relaxation $G_R(t)$ (or creep) functions are chosen to represent viscoelastic behavior. In the case of the FC model, these functions can be taken as power law kernel similar to Eq. (2) as,

$$G_R(t) = \frac{G_{\alpha}t^{-\alpha}}{\Gamma(1-\alpha)}; \qquad K_R(t) = \frac{K_{\beta}t^{-\beta}}{\Gamma(1-\beta)} \tag{13}$$

where K_{β} and G_{α} are bulk and shear relaxation moduli, respectively, while β and α are real numbers indicating the orders of bulk and shear power laws. Considering a time-independent bulk modulus $K_R(t) = K^{\upsilon}$, now, the strain–stress relationship can be given from Eq. (3) as:

$$\bar{\sigma}(t) = \int_0^t R(t-\tau)\dot{\epsilon}(\tau)\mathrm{d}\tau = K^{\upsilon}\theta + \frac{2G_{\alpha}}{\Gamma(1-\alpha)}\int_0^t (t-\tau)^{-\alpha}\dot{e}(\tau)\mathrm{d}\tau \tag{14}$$

The time-dependent shear relaxation modulus $G(t)$ is found via elastic/visco-elastic correspondence principle and inverse Laplace transform using the Mittag-Leffler special functions as given in Alotta et al. (2018a) and Bonfanti et al. (2020). The deviatoric stress tensor $\bar{\sigma}_{dev}$ can be written with shear relaxation function G_{α} and α as follows:

$$\bar{\sigma}_{dev}(t) = 2\left[\frac{G_{\alpha}}{\Gamma(1-\alpha)}\int_0^t (t-\tau)^{-\alpha}\dot{e}(\tau)\mathrm{d}\tau\right] = 2G_{\alpha}D^{\alpha}_t e(t) \tag{15}$$

Other fractional derivatives models exist, such as Riemann–Liouville fractional derivatives, Atangana–Baleanu fractional derivatives, Riesz derivatives, and others (Baleanu et al., 2012), but we refer here to the more classical one. The Caputo fractional derivative of any function $f(t)$ can be given by using the Grunwald–Letnikov (GL) fractional derivative (Wei and Shimizu, 2001; Schmidt and Gaul, 2002). The Grunwald–Letnikov approximation of the fractional derivative at the current time $n+1$ for a time step of Δt, $D^{\alpha}f(t^{n+1})$ for a generic f function (Samko et al., 1993) is:

$$D^{\alpha}f(t) = (\Delta t)^{-\alpha}\sum_{j=0}^{n} c_{j+1}(\alpha)f^{n+1-j} = (\Delta t)^{-\alpha}\left[f^1|\ldots|f^{n+1}\right]\begin{pmatrix} c_{n+1}(\alpha) \\ \vdots \\ c_1(\alpha)\end{pmatrix} \tag{16}$$

where the coefficients $c_j(\alpha)$ are defined by the recursive formula:

$$c_j(\alpha) = \begin{cases} \frac{(j-1-\alpha)}{j}c_{j-1}(\alpha) & \text{if} \quad j > 1 \\ 1 & \text{if} \quad j = 1 \end{cases} \tag{17}$$

Following this, the deviatoric stress $\bar{\sigma}_{dev}(t)$ at time $n+1$ for a time step Δt can be written in the form differential operators as:

$$\bar{\sigma}_{dev}(t) = 2G_{\alpha}D^{\alpha}_t e(t) = 2G_{\alpha}(\Delta t)^{-\alpha}\sum_{j=0}^{n} c_{j+1}(\alpha)e^{n+1-j} \tag{18}$$

Coefficients are such that $c_j(\alpha) < c_{j+1}(\alpha) < 0$ for $j > 1$ and $\lim_{j\to+\infty} c_j(\alpha) = 0$. In the FEM discretization, the f matrix stores the values of deviatoric strains e of previous time steps into columns $\left[\mathrm{e}^1|\ldots|\mathrm{e}^{n+1}\right]$ of increasing order, which act as the memory of the material. Using Eq. (14) with the volumetric and the deviatoric creep/relaxation functions are both well fitted by pure power-law function. Then their behavior can be reproduced by the spring pot model. In many cases of engineering cases, spring pots may not adequately reproduce the time-dependent features of viscoelastic materials completely, then other fractional viscoelastic material models with different combinations of springs along with spring pots are used (Alotta et al., 2018a).

3.3. Numerical implementation

In this section, the finite element implementation of the developed viscoelastic constitutive laws is briefly explained. We have implemented models into an implicit (Newton–Raphson) scheme; all of the stress components must be provided at the end of a previous time step. Here, we show details of the implementation of PS and FC models in a user element routine (UEL) of the finite element analysis program (FEAP) (Taylor, 2014). For the implementation of viscoelasticity in an implicit integration scheme, all the components of stress and the Jacobian at the end of a time step must be provided for each Gauss

point. The deviatoric and hydrostatic parts of the stress tensor are given by:

$$\bar{\sigma}_{dev}(t) = 2\left[G_\infty e(t) + \sum_{i=1}^{N}\left(G_i \exp\left(-\frac{\Delta t}{\tau_i}\right) h^i_{n+1}\right)\right]$$
$$= 2G_\alpha D^\alpha_t e(t); \qquad \bar{\sigma}_{vol}(t) = K^v\theta \tag{19}$$

The weak form corresponding to the energy functional Eq. (5) is derived by multiplying it by a virtual displacement v and integrating the result on the domain Ω. Applying the divergence theorem:

$$\int_\Omega \bar{\sigma}_{dev} e(u) : \varepsilon(v)\,\mathrm{d}\Omega + \int_\Omega K^v \mathrm{div}(u)\cdot\mathrm{div}(v)\,\mathrm{d}\Omega$$
$$= \int_\Omega f_v \cdot v\,\mathrm{d}\Omega + \int_{\partial\Omega} \bar{\mathrm{t}}\cdot \mathrm{v}\,\mathrm{d}\partial\Omega \tag{20}$$

Following discretization of Ω into elements such that $\Omega \to \Omega_e$. The trial solution functions space for displacement v can be defined as,

$$\mathcal{U}_h(u) = \left\{u \in H^1(\Omega) | \nabla u \in L^2(\Omega); u = u_d \text{ on } \partial\Omega_d\right\} \tag{21}$$

Respective test functions space for displacement v can be given as,

$$\mathcal{V}_h(v) = \left\{v \in H^1(\Omega) | \nabla \delta u \in L^2(\Omega); v = 0 \text{ on } \partial\Omega_d\right\} \tag{22}$$

For the single element, displacement and its gradients are approximated by Galerkin's method as follows,

$$u_e \approx N_u d_u, \quad \nabla u_e \approx B_u d_u, \quad v_e \approx N_u d_v, \quad \nabla v_e \approx B_u d_v, \tag{23}$$

where d_u are vectors of nodal values of displacements in our implementation, and the standard bi-linear shape functions N are used for both displacements and phase field variables. For simplicity, the gradient of the shape functions ∇N is denoted as B. Through the insertion of the previous interpolation formulae for the displacement and the phase field variables, the discrete versions of element residual vectors for both fields are given by

$$R_u = \int_{\Omega_e} \nabla v^T\left(\bar{\sigma}_{dev} + \bar{\sigma}_{vol}\right)\mathrm{d}\Omega - \int_{\Omega_e} v^T f\,\mathrm{d}\Omega - \int_{\partial\Omega_e} v^T \bar{t}\,\mathrm{d}\partial\Omega \tag{24}$$

To obtain the solutions for which $R_u = 0$ and because the corresponding residuals are nonlinear, an incremental-iterative scheme using the Newton–Raphson method is employed:

$$(\mathrm{d}u)_{t+\Delta t} = (\mathrm{d}u)_t - \left[K^u\right]^{-1}(R_u)_t \tag{25}$$

where coefficients of K^u are:

$$K^u = \frac{\partial R_u}{\partial d_u} = \int_\Omega B_v^T \bar{\mathbb{C}}^{vis} B_u \mathrm{d}\Omega \tag{26}$$

and $\bar{\mathbb{C}}^{vis}$ is the viscoelastic material tensor defined as

$$\bar{\mathbb{C}}^{vis} = \frac{\partial \Delta\sigma^{n+1}_{ij}}{\partial \Delta\varepsilon^{n+1}_{kh}} = \left(K^v - \frac{2}{3}G_{vis}\right)\delta_{ij}\delta_{kh} + G_{vis}\left(\delta_{ik}\delta_{jh} + \delta_{ih}\delta_{jk}\right) \tag{27}$$

The components of the material tensor are evaluated as follows:

$$\frac{\partial \Delta\sigma^{n+1}_{ii}}{\partial \Delta\varepsilon^{n+1}_{ii}} = K^v + \frac{4}{3}G_{vis},\ i = 1,2,3 \tag{28}$$

$$\frac{\partial \Delta\sigma^{n+1}_{ii}}{\partial \Delta\varepsilon^{n+1}_{jj}} = K^v - \frac{2}{3}G_{vis},\ i,j = 1,2,3;\ i \neq j \tag{29}$$

$$\frac{\partial \Delta\sigma^{n+1}_{ij}}{\partial \Delta\varepsilon^{n+1}_{ij}} = G_{vis},\ i,j = 1,2,3,\ i \neq j \tag{30}$$

where K^v is the time-independent bulk modulus and $G_{vis} = G_\infty + \sum_{i=1}^{N} G_i h_{\mathrm{vis}}$ and $G_{vis} = G_\alpha \Delta t^{-\alpha}$ for PS and FC models, respectively. The symbol δ is the Kronecker delta function. It can be noted that for both models the Jacobian depends only on the value of Δt and on the mechanical parameters. Fixed time-step increment Δt is considered to obtain convergence results. As compared to the PS model, which only requires the history of stress at the previous time step, the FC model needs a complete history of stresses at a Gauss point to calculate the stress at the current time step, which takes a significant amount of memory data. This is one of the main reasons the FC model takes a more extensive simulation time than the PS model. In order to reduce the amount of memory, one can use a larger time increment Δt or truncate the memory of the material for the GL derivative. In this study, we have chosen an optimum value for Δt to improve computational effectiveness.

4. Parameter identification procedure

Since the models for the viscoelastic material characterization were established in the previous section, here we describe how the material parameters' identification is performed. Among the various techniques suggested in the literature (Chen, 2000; Suchocki et al., 2013), a suitable choice is to exploit the relaxation response. For the relaxation test, a constitutive relation for the period of constant strain can be given as $\sigma(t) = E(t)\epsilon_0$, where $E(t)$ is the relaxation function and ϵ_0 is the strain at $t = 0$. Considering the material functions based on both the models can be given by expressions discussed previously as :

$$E(t) = A_\alpha t^{-\alpha}/\Gamma(1-\alpha), \qquad 0 \leq \alpha \leq 1, \text{FC Model} \tag{31}$$

$$E(t) = E_\infty + \sum_{j=1}^{N} E_j e^{-\frac{t}{\tau_j}}, \text{PS model} \tag{32}$$

where $R(t)$ is already available from experimental relaxation tests as given in Fig. 6. Consider a vector p which collects a set of model parameters $p = (p_1, p_2, \ldots, p_m)$, which are the unknown coefficients of the Prony series, or (A, α) for the FC model. Vector p takes values in the parameter space P, containing all the admissible values for p. This feasible set P also takes into account the restriction of model parameters. The problem of estimating the coefficients is addressed as an optimization problem which has the objective of minimizing cost function $\phi(p)$ defined as:

$$\phi(p) = \sum_{i=1}^{N}\left(f_i(p)\right)^2, \text{ for} f_i(p) = E_i^{\exp} - E_i^{\mathrm{model}}(p). \tag{33}$$

To minimize the cost function $\phi(p)$ there are various algorithms reported in the literature. Carollo et al. (2019) used the gradient descent algorithm and Particle Swarm Optimization (PSO) for identification. In Kraus et al. (2017), GUSTL was used to identify the Prony series from DMTA data, while parameters' estimation based on Genetic Algorithms (GA) was done in Kohandel et al. (2008). It was found that the Nonlinear Least Squares method based on the Levenberg–Marquardt optimization algorithm solves the minimization problem effectively (Ranganathan, 2004). Based on that, an interactive MATLAB program has been implemented to extract the model parameters from the present experimental relaxation tests. For the PS model, there are $2n + 1$ unknowns corresponding to E_∞, E_i's, and τ_i's. As the number of Maxwell's arms increases, so do the unknowns. In literature, it was suggested that the values for τ_i can be chosen as multiples of decades (Paggi and Sapora, 2015; Eitner, 2011). One of the reasons to choose multiple decades is to accommodate a complete relaxation response. For example $\tau = (10^0, 10^2, 10^4)$. In this way, PS model parameters would reduce to $n + 1$. The idea behind this is that every Maxwell's arm has a local impact on the shape of $E(t)$. Parameters τ_i define the range of the impact within time t and E_i sets the height of the model curve. As the problem gets constrained in the time range, a higher number of Maxwell's arms is needed to get an accurate response. Instead of fixing the time range τ_i's, the current study focuses on finding the optimum time τ_i for dashpots which can minimize the cost function $\phi(p)$. Though the total unknown model parameters are $2n+1$, the overall number of parameters to find gets reduced compared to fixing the time range. It also guarantees physical meaning to the outcome of the identification problem.

Fig. 10 shows the plot of $E(t)$ fitted with up to 5 Maxwell's Arms for a relaxation response for Lexan at 85 °C. For $n = 1$ to 3 Maxwell's arms,

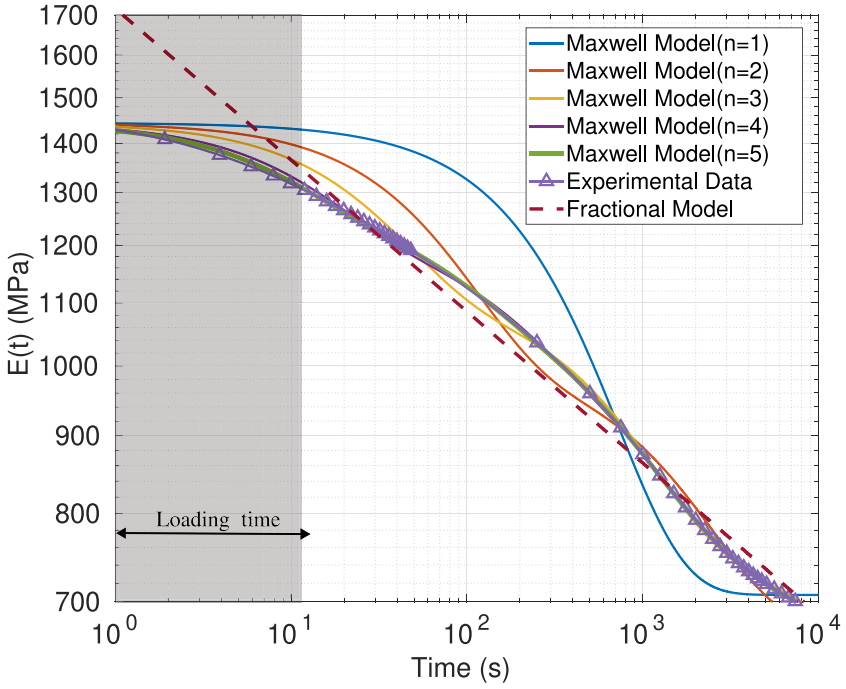

Fig. 10. Parameter estimation for relaxation response of Lexan at 85 °C for Maxwell and Fractional Model.

Table 5
Error analysis with increasing Maxwell's arm and with the Fractional Calculus Model.

Material Model	PS	1	2	3	4	5	FC
RSME Error (%)		123.320	12.896	0.887	0.101	0.014	1.301

the response of $E(t)$ is wavier, but as the number n of arms increases, the error between the experiment and model decreases as shown in Table 5.

Using the same algorithm, the FC model parameters A and α estimated for the relaxation response of Lexan are shown in Fig. 10. The response of the FC model is linear on the double logarithmic scale with an objective function, $y = \log \mathrm{E(t)}$, having a slope $m = -\alpha$ and a constant $c = \log \frac{A}{\Gamma(1-\alpha)}$. The initial value of the relaxation modulus depends on the constant. Since α is in line with the slope of relaxation, the corresponding values obtained from the FC model are higher than those from experimental data, but after a short duration, the FC model gives a very good fit as compared to the other Maxwell models with many arms.

The short-term period can be considered a loading time period most of the time (Glaesener et al., 2021), and it is time to obtain the constant state of stress, σ_0 for creep or a constant state of strain ϵ_0 as for relaxation experiments. Though the FC model is not able to predict short-time relaxation behavior, these models are very effective for long-term response (Bonfanti et al., 2020; Paggi and Sapora, 2015). Most PV modeling is done for a long-term response which accounts for the viscoelastic relaxation. These models are very effective since they require only two unknowns to describe the complete relaxation compared to $2n + 1$ for models based on the Prony series. All the experimental data along with the MATLAB code for estimating model parameters based on optimization is provided in Appendix, the supplementary data of this article.

4.1. Parameter estimation for temperature-dependent relaxation response of backsheet materials

The relaxation response of backsheet materials at different temperatures for constant strains can be modeled using PS and FC models, as shown in Fig. 11. The parameters for both material models are obtained for all backsheet materials based on the relaxation response stemming from experiments as shown in Tables 6 and 7, respectively. An optimum number of Maxwell's arms was identified, which was used to find parameters. As the number of PS parameters increases beyond 4–5 terms, finding the physical meaning of terms is difficult. But valid observations can be made from fractional calculus parameters. As temperature increases, the slope α increases until temperature reaches T_g, which is the glass transition temperature at which the constituent polymer material loses its crystalline phase. A similar analysis for EVA is available in (Paggi and Sapora, 2015) and (Eitner, 2011). As backsheet materials are layered composites, finding the exact transition temperature is difficult. T_g is helpful in finding Williams–Landel–Ferry (WLF) parameters of the theoretically expected shift function which plays an important role in Time-Temperature-Superposition-Principle (TTSP) to get an approximate response by shifting the master curve. Here we can estimate the approximate α from its variation corresponding to the temperature. Except for OSBS, for all other backsheet materials, α increases as temperature increases till higher temperatures around 65 °C, while for OSBS it starts decreasing from room temperature. One of the main reasons for having a lower α for OSBS relies on its lower T_g. Refer to Pander et al. (2011) and Eitner (2011) to understand the role of T_g on viscoelastic materials. Every time, it is not easy to get a master curve for viscoelastic materials such as backsheet, so performing temperature-dependent tests with characterization gives an idea about the change of material parameters with temperature.

4.2. Parameter estimation for strain-dependent relaxation response at constant temperature

The relaxation tests were performed on Lexan backsheet specimens keeping a constant temperature at different strain levels to understand

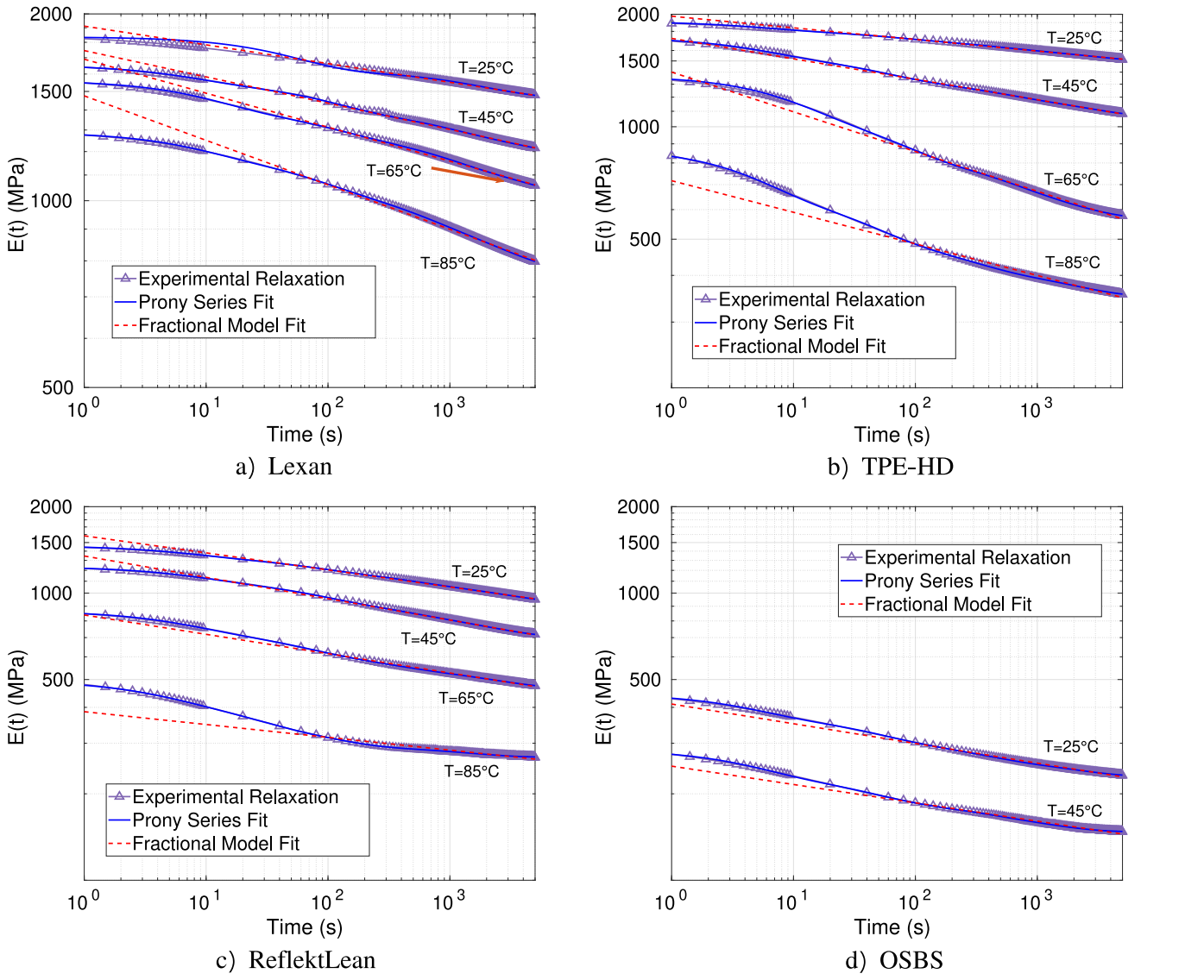

Fig. 11. Experimental results with numerical fitting for elastic relaxation modulus $E(t)$ versus time response for (a) Lean and, (b) OSBS backsheet materials at different temperatures.

the effect of strains on the relaxation curve. Fig. 12 shows the relaxation response modeled using PS and FC models for constant strains $\epsilon_c = 0.0167, 0.0250$, and 0.0333, for Lexan at 85 °C. The model parameters for both material models are obtained for all backsheet materials based on the relaxation response from experiments as shown in Table 8. It is noted that at 85 °C, specimens loaded at small strains relax early compared to those loaded at higher strains. No significant change in α was observed, so one may take a constant relaxation pattern for all strains at a constant temperature for Lexan. In most numerical simulations, taking constant α describing relaxation behavior for a given temperature is helpful. Similarly, for the PS series model, which is modeled with 4 arms, relaxation time τ_i and elastic stiffness E_i of respective arms seem to be in the same range, which can be taken as constant.

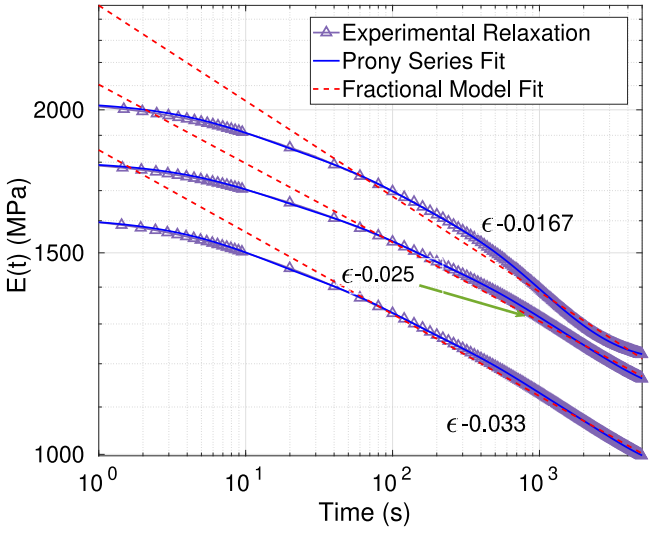

Fig. 12. Plot for relaxation response $E(t)$ of Lexan at 85 °C for Maxwell and Fractional Model for different strains.

5. Numerical analysis

This section implements models with parameters identified as in the previous section into a novel FEAP user element. They are applied here to some relevant case studies to prove their effectiveness in capturing experimental trends. Moreover, the numerical models are exploited to simulate realistic conditions for a PV module. Namely, we consider

Table 6
Material parameters identified based on prony series (PS) model.

Material	Temperature (°C)	Strain ε	PS Terms	Parameters Identified E_i (MPa), τ_i (s)	RSME Error (%)
OSBS	25	0.02	4	$E_\infty = 229.47,\ E_1 = 71.53,\ \tau_1 = 4.59$ $E_2 = 64.54,\ \tau_2 = 42.60,\ E_3 = 44.051$ $\tau_3 = 288.602,\ E_4 = 36.59,\ \tau_4 = 1980.18$	1.58
	45	0.02	4	$E_\infty = 147.48,\ E_1 = 51.264,\ \tau_1 = 4.85$ $E_2 = 44.41,\ \tau_2 = 39.26,\ E_3 = 16.66$ $\tau_3 = 267.65,\ E_4 = 25.38,\ \tau_4 = 1201.95$	1.01
TPE-HD	25	0.02	4	$E_\infty = 1490.58,\ E_1 = 99.523,\ \tau_1 = 5.431$ $E_2 = 92.24,\ \tau_2 = 57.21,\ E_3 = 91.41$ $\tau_3 = 373.25,\ E_4 = 141.17,\ \tau_4 = 2881.27$	2.23
	45	0.02	5	$E_\infty = 1058.275,\ E_1 = 106.69,\ \tau_1 = 3.10$ $E_2 = 134.925,\ \tau_2 = 15.96,\ E_3 = 163.601$ $\tau_3 = 67.19,\ E_4 = 116.425989,\ \tau_4 = 447.94$ $E_5 = 155.86,\ \tau_5 = 2813.216$	0.125
	65	0.02	4	$E_\infty = 567.25,\ E_1 = 268.456,\ \tau_1 = 10.4$ $E_2 = 258.15,\ \tau_2 = 64.9,\ E_3 = 136.014$ $\tau_3 = 463.862,\ E_4 = 138.82,\ \tau_4 = 1948.052$	2.06
	85	0.02	4	$E_\infty = 351.01,\ E_1 = 211.414,\ \tau_1 = 5.13$ $E_2 = 156.97,\ \tau_2 = 38.81,\ E_3 = 87.39$ $\tau_3 = 238.517,\ E_4 = 67.53,\ \tau_4 = 1987.01$	1.87
RefelektLean	25	0.02	4	$E_\infty = 921.77,\ E_1 = 118.23,\ \tau_1 = 7.15$ $E_2 = 127.92,\ \tau_2 = 61.44,\ E_3 = 120.61$ $\tau_3 = 372.49,\ E_4 = 174.36,\ \tau_4 = 2886.36$	0.485
	45	0.02	4	$E_\infty = 703.55,\ E_1 = 123.26,\ \tau_1 = 8.075$ $E_2 = 152.68,\ \tau_2 = 70.38,\ E_3 = 99.89$ $\tau_3 = 340.73,\ E_4 = 157.29,\ \tau_4 = 2096.87$	0.843
	65	0.02	4	$E_\infty = 466.78,\ E_1 = 120.22,\ \tau_1 = 6.97$ $E_2 = 121.301,\ \tau_2 = 54.067,\ E_3 = 72.56$ $\tau_3 = 273.29,\ E_4 = 85.613,\ \tau_4 = 2298.70$	1.53
	85	0.02	4	$E_\infty = 267.90,\ E_1 = 63.677,\ \tau_1 = 4.27$ $E_2 = 77.15,\ \tau_2 = 20.68,\ E_3 = 60.66$ $\tau_3 = 96.44,\ E_4 = 25.63,\ \tau_4 = 1423.905$	1.085
Lexan	25	0.0417	5	$E_\infty = 1355.09,\ E_1 = 95.945,\ \tau_1 = 9.38$ $E_2 = 92.683,\ \tau_2 = 85.95,\ E_3 = 78.51$ $\tau_3 = 534.650,\ E_4 = 80.385,\ \tau_4 = 2891.94$ $E_5 = 133.992,\ \tau_5 = 25430.43$	0.3318
	45	0.0417	4	$E_\infty = 1160.15,\ E_1 = 102.074,\ \tau_1 = 7.486$ $E_2 = 148.61,\ \tau_2 = 99.854,\ E_3 = 117.735$ $\tau_3 = 901.367,\ E_4 = 126.03,\ \tau_4 = 6086.96$	3.40
	65	0.0417	4	$E_\infty = 996.04,\ E_1 = 153.49,\ \tau_1 = 11.84$ $E_2 = 122.07,\ \tau_2 = 96.92,\ E_3 = 142.25$ $\tau_3 = 860.72,\ E_4 = 147.93,\ \tau_4 = 5758.89$	0.9792
	85	0.0417	5	$E_\infty = 603.52,\ E_1 = 170.69,\ \tau_1 = 10.88$ $E_2 = 165.59,\ \tau_2 = 93.78,\ E_3 = 209.43$ $\tau_3 = 686.34,\ E_4 = 169.95,\ \tau_4 = 1976.20$ $E_5 = 125.12,\ \tau_5 = 24459.21$	1.366

Table 7
Material parameters identified based on Fractional Calculus (FC) model.

Material	Temperature (°C)	Strain ε	α	A (MPa s^α)	RSME Error (%)
OSBS	25	0.02	0.06858	429.133	0.5364
	45	0.02	0.06390	259.943	0.6485
TPE-HD	25	0.02	0.03110	2013.616	0.169
	45	0.02	0.054732	1783.832	0.155
	65	0.02	0.106298	1503.640	0.558
	85	0.02	0.084548	757.535	0.828
ReflektLean	25	0.02	0.059327	1643.10	0.3313
	45	0.02	0.074289	1412.195	0.3329
	65	0.02	0.067308	875.67	0.407
	85	0.02	0.044636	397.10	1.067
Lexan	25	0.0417	0.030154	1946.379	0.1412
	45	0.0417	0.042348	1791.409	0.2087
	65	0.0417	0.054757	1749.269	0.3227
	85	0.0417	0.099548	1833.933	1.3014

Table 8
Parameter estimation for relaxation response of Lexan at 85 °C for Maxwell and Fractional Model for different strains.

Strain	A	α	E_0	E_1, τ_1	E_2, τ_2	E_3, τ_3	E_4, τ_4
				(MPa, s)			
0.0167	2605.01	0.0834	1211.33	146.03 9.08	190.78 73.87	226.27 593.06	261.85 1629.53
0.0250	2198.51	0.0689	1131.55	122.84 9.84	151.76 79.35	146.55 480.78	251.65 2477.23
0.0330	1930.74	0.0716	966.17	129.15 9.09	153.35 70.75	139.36 438.32	223.35 2562.24

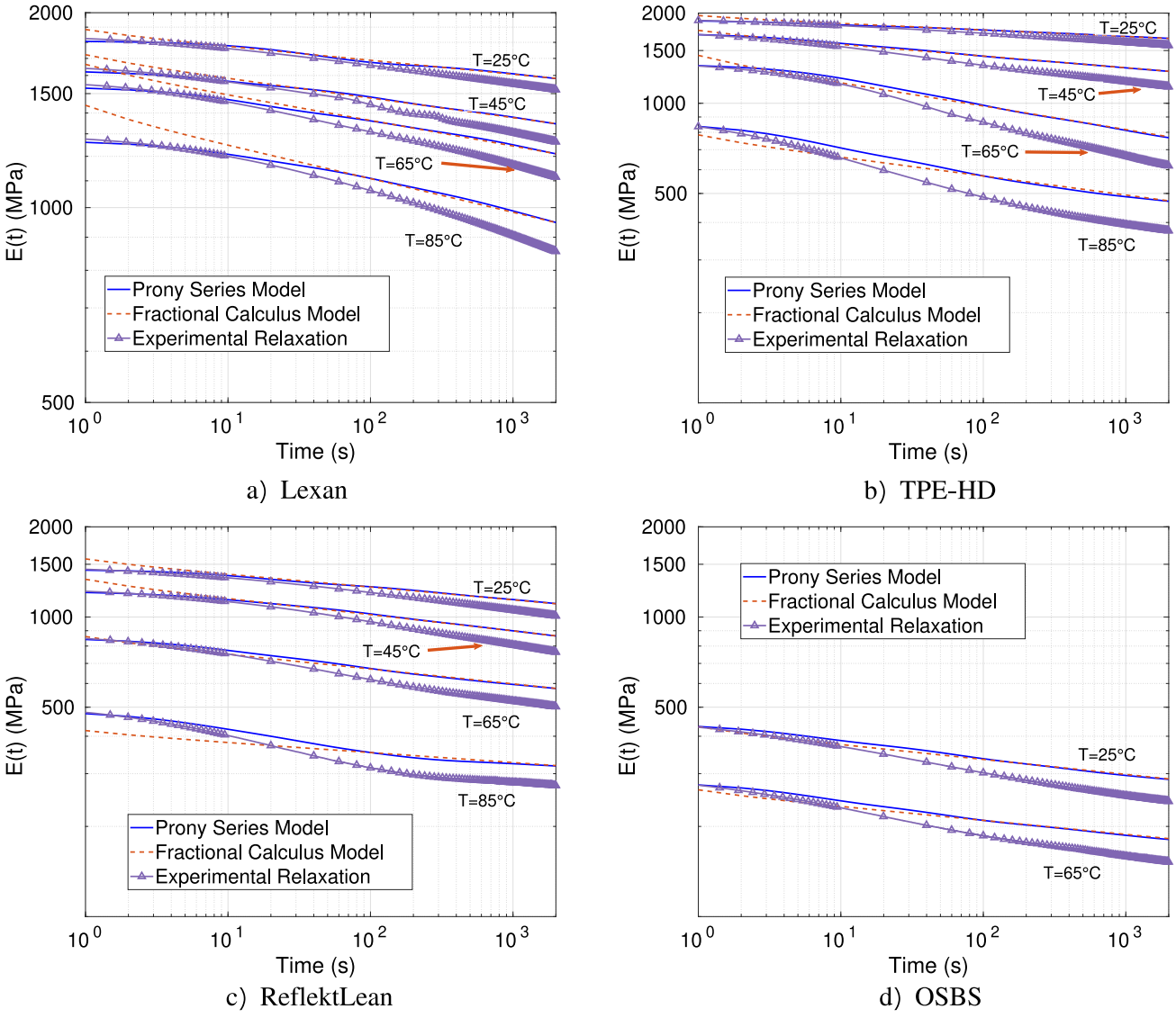

Fig. 13. Numerical results obtained from the simulations for elastic relaxation modulus $E(t)$ versus time.

bending tests to assess how the viscoelastic properties of the backsheet affect the axial stress σ_z along the PV module cross-section.

5.1. Numerical validation of relaxation tests

Numerical simulation of relaxation tests was performed on specimens of dimensions 50 mm × 20 mm × thickness of the respective backsheets. The bottom side is fixed, while the top side is subjected to constant displacement so that $\epsilon_0 = d/l_0$. The considered strain data for each material are collected in Table 3. The inertia of the material is neglected. Material parameters have already been estimated from experimental relaxation tests on different backsheets in the previous Section 4. Other input parameters besides the relaxation modulus are the Poisson's ratio $\nu = 0.30$ and the time-independent bulk modulus $K = E/3(1-2\nu)$. The PS and FC models show good convergence for a fixed time increment $\Delta t = 1$ s. Fig. 13 shows the numerically predicted elastic relaxation response of backsheet materials as compared to experimental results. The elastic relaxation modulus can be evaluated as $E(t) = \sigma(t)/\epsilon_0$, where $\sigma(t)$ is the nominal stress at time t predicted by numerical simulations. The numerical results for different backsheet

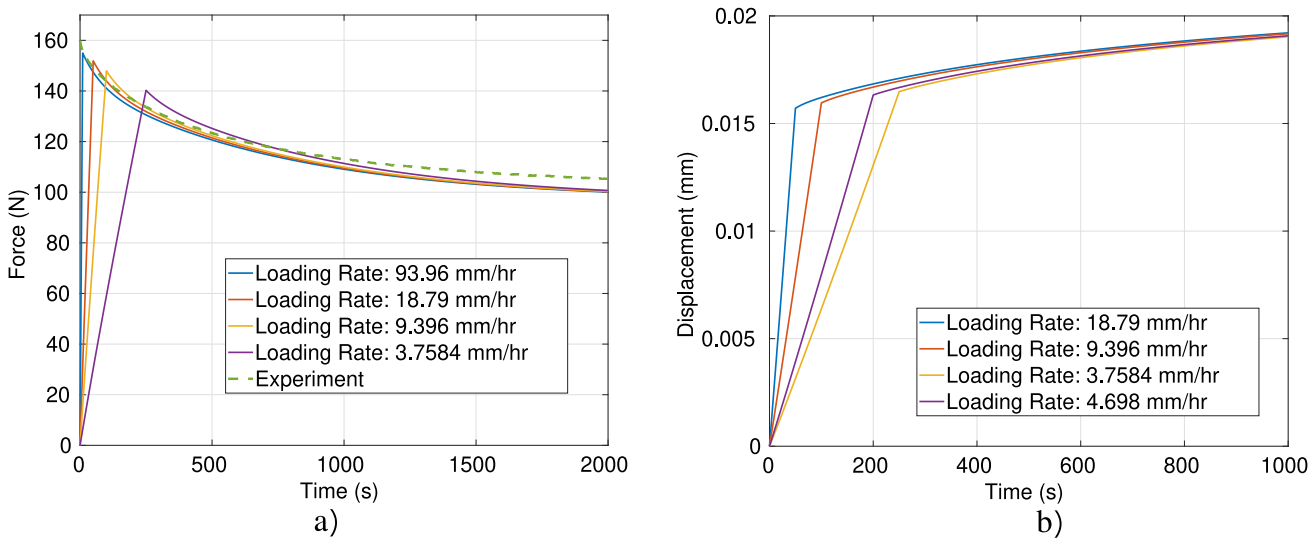

Fig. 14. Numerical results from simulations for the effect of strain rates on (a) Relaxation and (b) Creep response of Lexan backsheet at 85 °C considering 5 Maxwell arms.

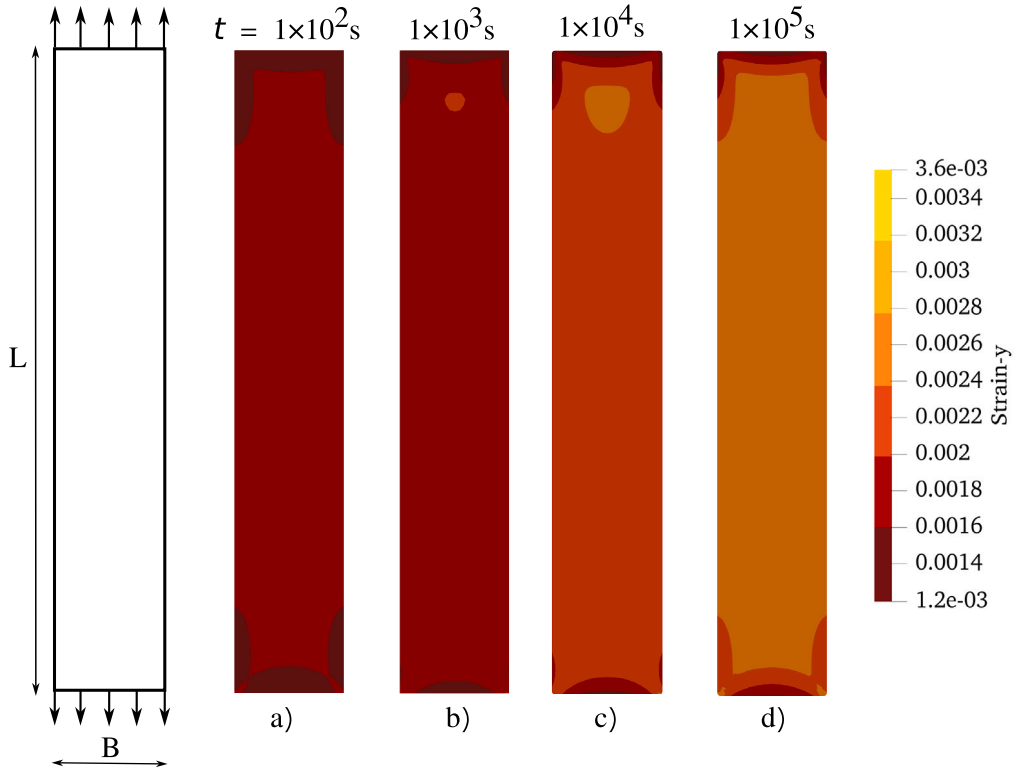

Fig. 15. Simulation of Lexan backsheet creep experiment at 25 °C: contour plot of the tensile strain at different points and its evolution in time.

materials are in good agreement with the outcome of experimental tests. The slight deviations from experimental results can be ascribed to a time-independent bulk modulus assumption.

5.2. Effect of the initial loading rate on creep and relaxation experiments

To understand the effect of the initial loading rate on elastic relaxation and creep of materials, a numerical study is performed with a different initial loading rate for the Lexan backsheet. A specimen of dimensions 60 mm × 40 mm × 0.296 mm is clamped on the bottom side and loaded on top with a constant strain $\epsilon = 0.0065$ over the period of the relaxation test, while a constant force $F = 30$ N is maintained over time for the creep tests. The numerical results with the 5 Prony Series arm model are shown in Fig. 14. It can be observed that the initial loading rate significantly affects the initial stress σ_0 or strain ϵ_0. But, over time, both relaxation and creep responses with varying initial loading rates converged together as we kept all input material parameters constant. From those plots, it is evident that the initial loading rate does not affect the long-term response. Fig. 15 shows a specimen's numerically predicted creep behavior at 25 °C with

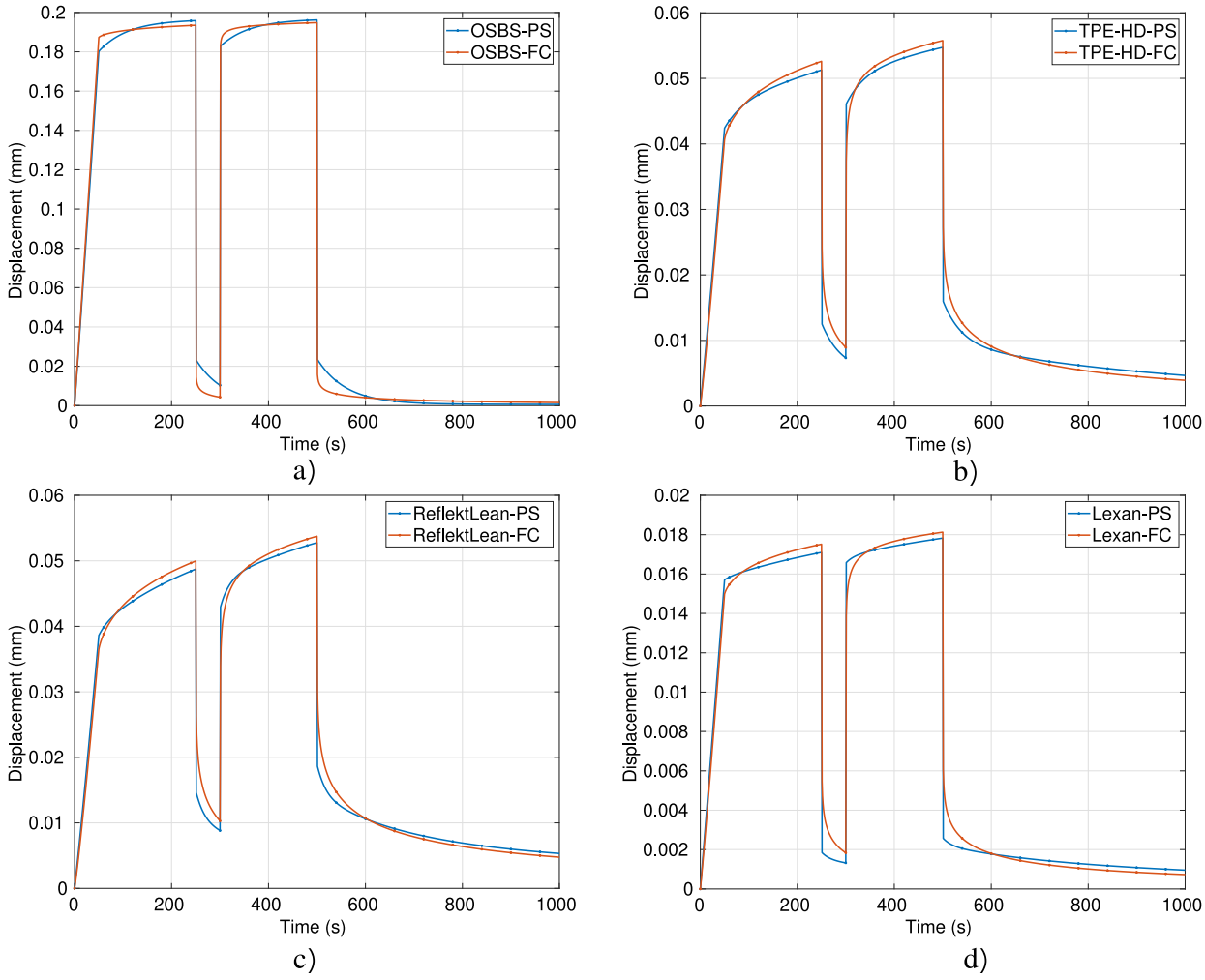

Fig. 16. Response of backsheet materials (a) OSBS, (b) TPE-HD, (c) ReflektLean, and (d) Lexan under creep cyclic loading at 25 °C.

dimensions $L = 120$ mm, $B = 20$ mm, and 0.296 mm thick Lexan backsheet subjected to the constant $F = 40$ N. The contour plot of the axial strain ϵ_l over a time period from 100 to 10,000 s is shown. The predicted spatial variation of strain is the same in both viscoelastic models.

5.3. Response under creep cycles

A numerical investigation is performed to understand the response of backsheet materials, with parameters identified in Table 6, when subjected to creep cycles as in Fig. 16. A specimen of dimensions 60 mm × 40 mm × thickness is clamped on the bottom side and loaded on top. All materials were subjected to the constant traction $F = 30$ N over the first 200 s, relaxed for the next 50 s, and again loaded with constant $F = 30$ N for another 200 s period, followed by unloading for the rest of the time. The response of both material models, and for all the backsheet materials, is shown in Fig. 16. Both PS and FC material models show good predictions. It also shows that FC models with only two unknown parameters are able to predict responses very well as PS models with a much larger number of unknowns. As OSBS has a lower elastic modulus than the other materials, it deforms more than the others, and it also gets faster relaxed. An important observation that can be made from all the material responses is that, after the first cycle of loading, the material deforms more at the next cycle for the same load, as compared to the first one. This is primarily due to the polymeric response of backsheet materials, as chains of constituent polymers get unstrained and stretched over the first cycle, followed by relaxation. This response is very important in the case of failures of PV modules that are repeatedly subjected to cyclic loads.

5.4. Three-point bending of a PV mini-module

In this section, using the identified model parameters given in Table 6, the response of a PV mini-module under bending is being tested for a long duration of time to understand the effect of viscoelastic properties of the backsheet in terms of axial stresses σ_z developed within the PV module. The PV mini-module under study is composed of the following layers (from the intrados to the extrados): a backsheet 0.32 mm thick, an EVA layer with $E_{\text{EVA}} = 10$ MPa 0.5 mm thick, a polycrystalline Si solar cell with $E_{\text{Si}} = 130$ GPa 0.166 mm thick, another EVA layer 0.5 mm thick, and finally a PET with $E_{\text{PET}} = 2800$ MPa cover 0.265 mm thick. The span of the mini-module is $L = 180$ mm. The three-point bending experiment and boundary conditions are schematically shown in Fig. 17.

Following the experimental tests performed by Borri et al. (2018), the PV mini-module was subjected to a maximum deformation of 20 mm at its mid-span position, which led to a reaction force of 64 N. The experimental setup is shown in Fig. 18. In the FE analysis, Poisson's ratio ν is taken as 0.3 for all layers, assuming that all layers are perfectly bonded. The time-dependent response of backsheet materials is introduced based on the elastic moduli values at 85 °C, as given in Table 2.

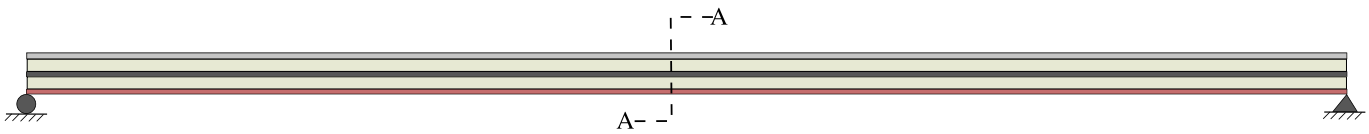

Fig. 17. Schematic showing three-point bending of a PV mini-module.

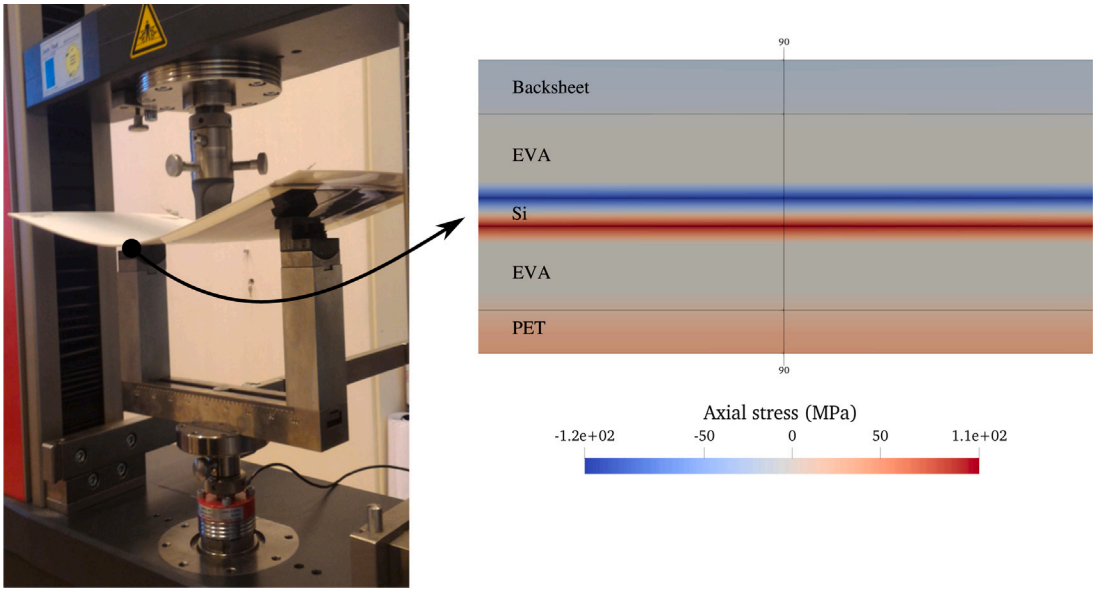

Fig. 18. (a) The experimental setup for the bending test for PV laminate (Borri et al., 2018), and (b) Axial stress σ_z(MPa) across the mid-cross-section of the PV mini-module under constant displacement $u_y = -20$ mm with Lexan backsheet at 85 °C.

The PV mini-module is subjected to a constant mid-span defection of $u_y = -20$ mm over the whole time period. As correspondence principle (Alotta et al., 2018a) proved to be valid for linear viscoelasticity, the shape of the deformed configuration of the backsheet layer is the same as that with elastic one only difference being stress across the layer, which scales with time and directly affects stress configuration across whole PV module with time. The axial stress σ_z distribution for the PV module considering Lexan as backsheet material over time is shown in Fig. 18. The variation of stress σ_{BS} over time across a range of temperatures is shown in Fig. 19. It shows that σ_{BS} decreases as temperature increases. It can be observed that due to the reduction of $E(t)$ over time, higher stresses build up across the Si layer. Hence, the progressive degradation of elasticity of the backsheet may lead to mechanical failure of Si cells, which are thin and brittle.

6. Discussion and conclusion

In this study, the viscoelastic response of commercially available backsheet materials has been experimentally characterized for temperature-dependent relaxation and uniaxial tensile tests. An extensive viscoelastic experimental study on backsheet materials has been carried out, considering the temperature-dependent properties for characterizing the mechanical properties. Experiments showed that the Lexan backsheet has the highest strength compared to other back sheet materials under study. Based on an experimental campaign, we have proposed small-strain viscoelastic models based on the Prony-Series (PS) and Fractional Calculus (FC) models for constitutive equations. We have implicitly implemented both models as user element (UEL) subroutines in FEAP (Taylor, 2014). We have shown that the FC model can be implemented in finite elements by using the discretized version of the fractional derivative provided by Grunwald–Letnikov (GL) and the PS model through a semi-analytical approach. The current element formulation can be easily implemented with any FE code.

A robust optimization procedure for identifying viscoelastic material parameters has been devised for both models. It was observed that the FC model needs only two parameters, A and α, to characterize the relaxation response, while the PS model needs the identification of 7 to 11 unknown parameters to achieve analogous performance. It is also noted that FC models cannot predict the relaxation behavior for very short periods below 10^1 s. Still, they give very good predictions for the long-term response, which is the regime of interest for applications. FC models require the complete time history of strains as compared to the PS model, in which only the strain at a current and a previous time step is required. In this regard, the FC model needs more memory to store the history variables as compared to the PS model.

The parameters identified can be directly used as a material input for simulating the response of the respective backsheet materials. Following identifications of relevant material parameters, we have validated the model with the experimental data, showing good predictability. From the numerical experiments we also showed that when the material is loaded under creep cyclic loads, the material undergoes more deformation as long as the number of cycles increases.

Such an extensive experimental study and constitutive modeling will help the design and the simulation of a more comprehensive digital twin models of PV modules. To understand the effect of the viscoelastic response of the backsheets on the stress field inside a PV module, a three-point bending experiment was simulated with parameters identified for both viscoelastic material models. Numerical predictions show that the elastic modulus reduction over time of the backsheet material leads to an increase in the axial stress σ_z to be withstood by the Silicon layer, which may enhance the occurrence of brittle fracture in Silicon solar cells.

Future investigations will concern the fracturing of the PV backsheet, as shown in Fig. 20. In most cases, these failures occur due to material degradation over time. To address fracture in the backsheet, the present framework can be coupled with a phase field approach to

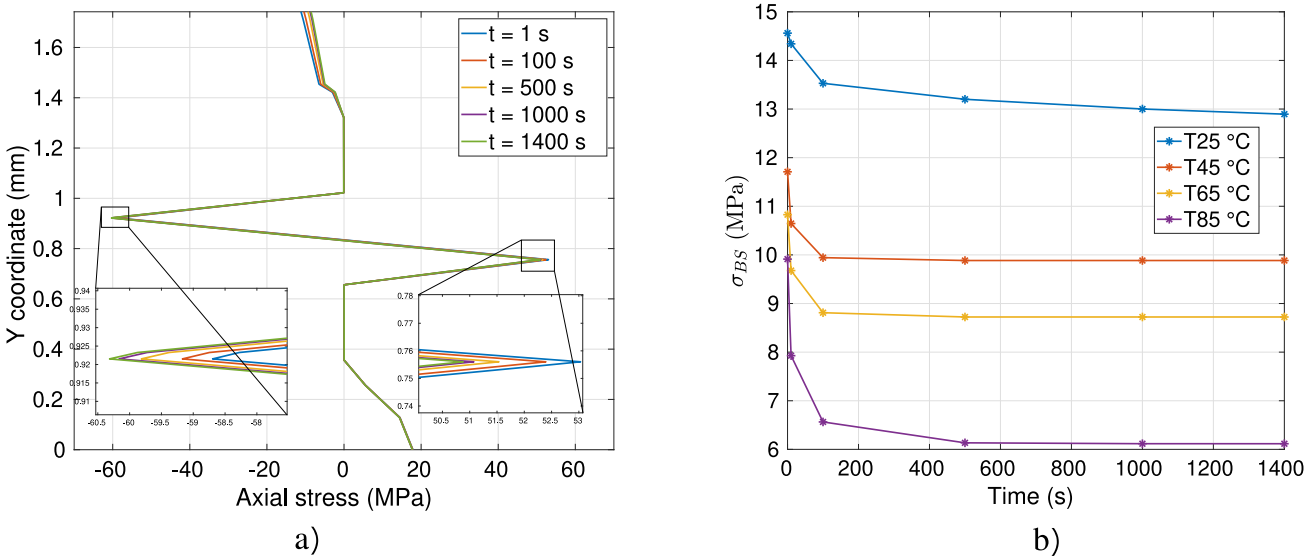

Fig. 19. (a) Axial stress σ_z(MPa) across the mid-cross-section of the PV mini-module under constant displacement $u_y = -20$ mm with Lexan backsheet at 85 °C, and (b) Variation of σ_{BS} (MPa) with respect to time over a different ranges of temperature when subjected to bending.

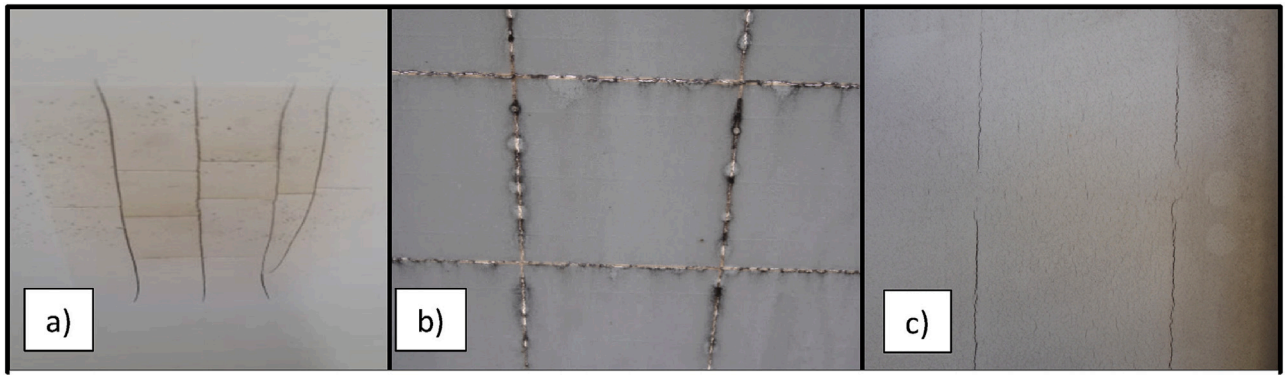

Fig. 20. Common failures in PV backsheet due to thermo-mechanical and material degradation: (a) cracked backsheet beneath a hot Si-cell, (b) squared cracks beneath cell interspaces, and (c) longitudinal cracks located beneath bus-bars, from Eder et al. (2019).

fracture, which could be effectively applied to simulate and capture such complex material-degradation scenarios.

CRediT authorship contribution statement

A.R. Dusane: Methodology, Software, Investigation, Experiments, Validation, Writing – original draft, Writing – review & editing. **P. Lenarda:** Software, Visualization, Writing – review & editing. **M. Paggi:** Conceptualization, Experiments, Supervision, Original draft, Writing – review & editing.

Declaration of competing interest

The authors declare that they have no known competing financial interests or personal relationships that could have appeared to influence the work reported in this paper.

Data availability

Data will be made available on request.

Acknowledgments

The authors acknowledge funding from the Italian Ministry of University and Research to the research project of national interest PRIN 2017 XFAST-SIMS: Extra fast and accurate simulation of complex structural systems (GA 20173C478N).

Appendix. Supplementary data

Supplementary data related to this article can be found at https://github.com/ardusane10

References

Agroui, K., Collins, G., Farenc, J., 2012. Measurement of glass transition temperature of crosslinked EVA encapsulant by thermal analysis for photovoltaic application. Renew. Energy 43, 218–223.

Alotta, G., Barrera, O., Cocks, A., Di Paola, M., 2018a. The finite element implementation of 3D fractional viscoelastic constitutive models. Finite Elem. Anal. Des. 146, 28–41.

Alotta, G., Barrera, O., Pegg, E.C., 2018b. Viscoelastic material models for more accurate polyethylene wear estimation. J. Strain Anal. Eng. Des. 53 (5), 302–312.

Baleanu, D., Diethelm, K., Scalas, E., Trujillo, J.J., 2012. Fractional Calculus: Models and Numerical Methods, Vol. 3. World Scientific.

Bonfanti, A., Kaplan, J., Charras, G., Kabla, A., 2020. Fractional viscoelastic models for power-law materials. Soft Matter 16 (26), 6002–6020.

Borri, C., Gagliardi, M., Paggi, M., 2018. Fatigue crack growth in silicon solar cells and hysteretic behaviour of busbars. Sol. Energy Mater. Sol. Cells 181, 21–29.
Bosco, N., Springer, M., He, X., 2020. Viscoelastic material characterization and modeling of photovoltaic module packaging materials for direct finite-element method input. IEEE J. Photovolt. 10 (5), 1424–1440.
Budday, S., Sommer, G., Holzapfel, G., Steinmann, P., Kuhl, E., 2017. Viscoelastic parameter identification of human brain tissue. J. Mech. Behav. Biomed. Mater. 74, 463–476.
Carollo, V., Piga, D., Borri, C., Paggi, M., 2019. Identification of elasto-plastic and nonlinear fracture mechanics parameters of silver-plated copper busbars for photovoltaics. Eng. Fract. Mech. 205, 439–454.
Chen, T., 2000. Determining Viscoelastic Strain Data a Prony Material Series for a from Time Varying. NASA Langley Research Center.
Czanderna, A., Pern, F., 1996. Encapsulation of PV modules using ethylene vinyl acetate copolymer as a pottant: A critical review. Sol. Energy Mater. Sol. Cells 43 (2), 101–181.
De Oliveira, M., Cardoso, A., Viana, M., Lins, V., 2018. The causes and effects of degradation of encapsulant ethylene vinyl acetate copolymer (EVA) in crystalline silicon photovoltaic modules: A review. Renew. Sustain. Energy Rev. 81, 2299–2317.
Dietrich, S., Pander, M., Sander, M., Schulze, S., Ebert, M., 2010. Mechanical and thermomechanical assessment of encapsulated solar cells by finite-element-simulation. In: Reliability of Photovoltaic Cells, Modules, Components, and Systems III, Vol. 7773. SPIE, pp. 117–126.
Eder, G., Voronko, Y., Oreski, G., Mühleisen, W., Knausz, M., Omazic, A., Rainer, A., Hirschl, C., Sonnleitner, H., 2019. Error analysis of aged modules with cracked polyamide backsheets. Sol. Energy Mater. Sol. Cells 203, 110194.
Eitner, U., 2011. Thermomechanics of photovoltaic modules [ph. d. thesis]. Zentrum für Ingenieurwissenschaften der Martin-Luther-Universität Halle-Wittenberg.
Fred-Ahmadu, O.H., Bhagwat, G., Oluyoye, I., Benson, N.U., Ayejuyo, O.O., Palanisami, T., 2020. Interaction of chemical contaminants with microplastics: principles and perspectives. Sci. Total Environ. 706, 135978.
Gagliardi, M., Lenarda, P., Paggi, M., 2017. A reaction-diffusion formulation to simulate EVA polymer degradation in environmental and accelerated ageing conditions. Sol. Energy Mater. Sol. Cells 164, 93–106.
Glaesener, R.N., Bastek, J.-H., Gonon, F., Kannan, V., Telgen, B., Spöttling, B., Steiner, S., Kochmann, D.M., 2021. Viscoelastic truss metamaterials as time-dependent generalized continua. J. Mech. Phys. Solids 156, 104569.
Henschke, O., Köller, F., Arnold, M., 1997. Polyolefins with high glass transition temperatures. Macromol. Rapid Commun. 18 (7), 617–623.
Hervy, M., Santmarti, A., Lahtinen, P., Tammelin, T., Lee, K.-Y., 2017. Sample geometry dependency on the measured tensile properties of cellulose nanopapers. Mater. Des. 121, 421–429.
Hirschl, C., Biebl-Rydlo, M., DeBiasio, M., Mühleisen, W., Neumaier, L., Scherf, W., Oreski, G., Eder, G., Chernev, B., Schwab, W., et al., 2013. Determining the degree of crosslinking of ethylene vinyl acetate photovoltaic module encapsulants – A comparative study. Sol. Energy Mater. Sol. Cells 116, 203–218.
Holzapfel, G.A., Simo, J.C., 1996. A new viscoelastic constitutive model for continuous media at finite thermomechanical changes. Int. J. Solids Struct. 33 (20–22), 3019–3034.
Kaliske, M., Rothert, H., 1997. Formulation and implementation of three-dimensional viscoelasticity at small and finite strains. Comput. Mech. 19 (3), 228–239.
Kim, J., Rabelo, M., Padi, S., Yousuf, H., Cho, E.-C., Yi, J., 2021. A review of the degradation of photovoltaic modules for life expectancy. Energies 14 (14), 4278.
Knauss, W., 2015. A review of fracture in viscoelastic materials. Int. J. Fract. 196 (1), 99–146.
Kohandel, M., Sivaloganathan, S., Tenti, G., 2008. Estimation of the quasi-linear viscoelastic parameters using a genetic algorithm. Math. Comput. Model. 47 (3-4), 266–270.
Kraus, M., Schuster, M., Kuntsche, J., Siebert, G., Schneider, J., 2017. Parameter identification methods for visco-and hyperelastic material models. Glass Struct. Eng. 2 (2), 147–167.
Lang, M., Oreski, G., Helfer, E., Halm, A., Klenk, M., Fuchs, P., 2022. FEM simulation of deformations and stresses in strings of shingled solar cells under mechanical and thermal loading. In: AIP Conference Proceedings, Vol. 2709, No. 1. AIP Publishing.
Lenarda, P., Paggi, M., 2022. A computational framework for rheologically complex thermo-visco-elastic materials. Int. J. Solids Struct. 236, 111297.
Liu, Z., Castillo, M., Youssef, A., Serdy, J., Watts, A., Schmid, C., Kurtz, S., Peters, I., Buonassisi, T., 2019. Quantitative analysis of degradation mechanisms in 30-year-old PV modules. Sol. Energy Mater. Sol. Cells 200, 110019.
Liu, Z., Reinoso, J., Paggi, M., 2022. A humidity dose-CZM formulation to simulate new end-of-life recycling methods for photovoltaic laminates. Eng. Fract. Mech. 259, 108125.
Londono, J.G., Berger-Vergiat, L., Waisman, H., 2016. A prony-series type viscoelastic solid coupled with a continuum damage law for polar ice modeling. Mech. Mater. 98, 81–97.
Marques, S., Creus, G., 2012. Computational Viscoelasticity. Springer Science & Business Media.
Omazic, A., Oreski, G., Halwachs, M., Eder, G., Hirschl, C., Neumaier, L., Pinter, G., Erceg, M., 2019. Relation between degradation of polymeric components in crystalline silicon PV module and climatic conditions: A literature review. Solar Energy Mater. Solar Cells 192, 123–133.
Omnexus, Glass transition temperature. https://omnexus.specialchem.com/polymer-properties/properties/glass-transition-temperature.
Ottersböck, B., Oreski, G., Pinter, G., 2022. How to accelerate natural weathering of polymeric photovoltaic backsheets–A comparison with standardized artificial aging. Sol. Energy Mater. Sol. Cells 244, 111819.
Paggi, M., Corrado, M., Berardone, I., 2016. A global/local approach for the prediction of the electric response of cracked solar cells in photovoltaic modules under the action of mechanical loads. Eng. Fract. Mech. 168, 40–57.
Paggi, M., Sapora, A., 2015. An accurate thermoviscoelastic rheological model for ethylene vinyl acetate based on fractional calculus. Int. J. Photoenergy 2015.
Pander, M., Dietrich, S., Schulze, S.-H., Eitner, U., Ebert, M., 2011. Thermo-mechanical assessment of solar cell displacement with respect to the viscoelastic behaviour of the encapsulant. In: 2011 12th Intl. Conf. on Thermal, Mechanical & Multi-Physics Simulation and Experiments in Microelectronics and Microsystems. IEEE, pp. 1–6.
Podlubny, I., 1999. Fractional Differential Equation. San Diego. Academic Press USA.
Polymerdatabse, Thermophysical properties of polymers. https://polymerdatabase.com/main.html.
Ranganathan, A., 2004. The levenberg-marquardt algorithm. Tutoral LM algorithm 11 (1), 101–110.
Reese, S., Govindjee, S., 1998. A theory of finite viscoelasticity and numerical aspects. Int. J. Solids Struct. 35 (26–27), 3455–3482.
Romer, P., Oreski, G., Beinert, A.J., Neuhaus, H., Mittag, M., 2020. More realistic consideration of backsheets coefficient of thermal expansion on thermomechanics of PV modules. In: Presented At the 37th European PV Solar Energy Conference and Exhibition, Vol. 7, No. 11.
Samko, S., Kilbas, A., Marichev, O., et al., 1993. Fractional Integrals and Derivatives, Vol. 1. Gordon and breach science publishers, Yverdon Yverdon-les-Bains, Switzerland.
Sánchez, E., Nájera, A., Sotomayor, O., 2022. Numerical study of the viscoelastic mechanical response of polystyrene in the process of thermoforming through the generalized maxwell model. Mater. Today Proc. 49, 107–114.
Scherer, R., Kalla, S.L., Tang, Y., Huang, J., 2011. The grunwald-letnikov method for fractional differential equations. Comput. Math. Appl. 62 (3), 902–917.
Schmidt, A., Gaul, L., 2002. Finite element formulation of viscoelastic constitutive equations using fractional time derivatives. Nonlinear Dynam. 29, 37–55.
Simo, J., 1987. On a fully three-dimensional finite-strain viscoelastic damage model: formulation and computational aspects. Comput. Methods Appl. Mech. Engrg. 60 (2), 153–173.
Suchocki, C., Pawlikowski, M., Skalski, K., Jasiński, C., Morawiński, L., 2013. Determination of material parameters of quasi-linear viscoelastic rheological model for thermoplastics and resins. J. Theoret. Appl. Mech. 51.
Taylor, R., 2014. FEAP-A Finite Element Analysis Program. Citeseer.
Taylor, R., Pister, K., Goudreau, G., 1970. Thermomechanical analysis of viscoelastic solids. Internat. J. Numer. Methods Engrg. 2 (1), 45–59.
Vázquez, M., Rey-Stolle, I., 2008. Photovoltaic module reliability model based on field degradation studies. Prog. Photovolt., Res. Appl. 16 (5), 419–433.
Wei, Z., Shimizu, N., 2001. FE formulation for the viscoelastic body modeled by fractional constitutive law. Acta Mech. Sinica 17 (4), 354–365.
Xu, Q., Engquist, B., 2018. A mathematical model for fitting and predicting relaxation modulus and simulating viscoelastic responses. Proc. R. Soc. A 474 (2213), 20170540.
Xu, Q., Solaimanian, M., 2009. Modelling linear viscoelastic properties of asphalt concrete by the huet–sayegh model. Int. J. Pavement Eng. 10 (6), 401–422.